LAPPEENRANTA UNIVERSITY OF TECHNOLOGY

Department of Physics

Technical Physics

Marina Elistratova

OPTICAL SPECTROSCOPY OF ORGANIC MATERIAL BASED ON C_{60}<A^2B^6>

Examiners: Professor Erkki Lähderanta

Professor Irina Zakharova

ABSTRACT

Lappeenranta University of Technology

Department of Physics

Technical Physics

Marina Elistratova

Optical spectroscopy of organic material based on $C_{60}<A_2B_6>$

Master's thesis

2015

56 pages, 38 figures and 6 tables

Examiners: Professor Erkki Lähderanta

Professor Irina Zakharova

Keywords: fullerene, thin films, photoluminescence, x-ray, quantum chemical calculations

The structure and optical properties of thin films based on $C_{60}<A^2B^6>$ materials are studied. Reproducible vacuum method of thin fullerene films production with Cd<Te;S> impurity on Si, glass and mica surfaces is developed. Surface morphology of the films are investigated by AFM and SEM methods. The ab initio quantum - chemical calculations of the geometry, total energy and excited energy states of complex fullerene- cadmium telluride supramolecules are performed. Photoluminescence spectra of composite thin films based on C_{60}<CdTe> before and after X-ray irradiation were measured. The intensity of additional peaks is defined as the charge composition due to the type of substrate. These results are interpreted as an appearance of the dipole-allowed transitions in the fullerene excited singlet states spectrum cause of an interference with cadmium telluride.

X-ray irradiated films were investigated, and additional peaks in photoluminescence spectra were detected. These peaks appear as a result of molecular complexes formation from C_{60}CdTe mixture and dimerization of the films. Density functional B3LYP quantum-chemical calculations for C_{60}CdTe, molecular complexes, $(C_{60})_2$ and $C_{120}O$ dimers were performed to elucidate some experimental results.

ACKNOWLEDGEMENTS

The main part of scientific work and publications have been done in Peter the Great Saint-Petersburg Polytechnic University. Some experiments were done in collaborations with Roman Dubrovin, Nicolay Romanov, Yulia Vainshtein and Oleg Kvyatkovskii from A. F. Ioffe Technical Institute, Russian Academy of Science, Saint-Petersburg.

I would like to express my grate gratitude to my scientific director at The Polytechnic University Irina Zakharova for help and support throughout the work.

I would like to express my highest appreciations and thanks to my LUT supervisor Professor Erkki Lähderanta for his work with students and support throughout the collaborations. Studying in LUT with him was pleasant and interesting.

I would like to express my gratitude to Lappeenranta University of Technology for possibility to graduate in Finland and for financial support.

I wish to thank my parents Galina and Anatoly for their care and help. I most warmly thank my husband Roman for scientific support and for love and happiness.

Lappeenranta, 2015

Elistratova Marina

CONTENTS

List of abbreviations

BHj bulk heterojunction

Chal chalcogenide atoms

DFT density of functional theory

E_g energy gap

Ec conductive band

Ev valence band

E_{vibr} vibrational energy

Hj heterojunction

PL photolominescense

QCV quasi-closed volume

QCC quantum chemical calculations

v_{abs} excited light frequency

Chapter 1

1 INTRODUCTION

1.1 Motivation for research

Organic/inorganic mixed nanocomposites promise to be valuable to solar energy conversion, photovoltaics, specifically to novel light-driven systems [Shibu, E. S et al (2012)]. Particularly, new composite materials based on C_{60} fullerene as well as nonorganic semiconductor nanoparticles A_2B_6 are in a great interest [Bang, J. H., & Kamat, P. V. (2011)]. Properties of hybrid materials may be regulated via a variety of functional groups, which can be incorporated in the organic C_{60} matrix. Photovoltaic devices, sensors, optoelectronics, etc. might represent some of the most important applications of these novel materials. In this work thin films of new hybrid organic-inorganic semiconductors, exhibiting photoconductive properties have been produced by simple vacuum method. Molecular semiconductor materials have been studied for more than a half century because they have high potential for unique device applications such as light-emitting diodes, solar cells, and field-effect transistors with low cost, low weight, and mechanically flexible electronics. Therefore, the development of composite electronic and photoelectronic materials and structures based on C_{60} is relevant and important. In the last years, many studies have been focused on optical characteristics of both C_{60} molecules and solid fullerite.

1.2 Choosing of $C_{60}<A^2B^6>$ material

Frenckel excitons formation takes place as a result of photons absorption by C_{60} molecule. These excitons are singlet excitation of C_{60} molecule, which quickly recombine in triplet excite state. It is necessary to separate excitons to get photovoltage. Heterojunction of donor and acceptor materials may observe this function very effective. It holds with charge transfer mechanism between molecules. It was found that fullerene C_{60} is a good electron acceptor. Conjugated polymers, phthalocyaniness, materials from porphyrin class and also nonorganic semiconductors from A^2B^6 group are effective donors. Fulleren triplet excitation expends on C_{60} anion or cation donor formation because of C_{60} molecule and donor molecule interactions. Any other, effective Frenckel excitons separation on electron and hole takes place. Therefore, this material contacts with fullerene are the ones on which the research is focused as a possible material for affective solar elements creation. Nevertheless, the main

property, which has to be taken into account when we use organic structures, is their quick degradation under the influence of oxygen or H_2O vapor. This aspect reduces to comparatively short useful time of those devices. Consequently, intensive research in the field of composite organic and nonorganic semiconductor, which includes C_{60}-CdTe films, structures is underway. It is done to increase the lifetime of organic solar cells. CdTe is a well-known material for photovoltaic because it is a direct-gap semiconductor with 1.5 eV energy band gap, which corresponds with 820 nm wavelength. This band gap is optimal for absorption of sunlight, because increase of the band gap leads to the decrease of the solar spectrum coverage. Decreasing bang gap lead to leaving of a significant portion of absorbed photons to intraband scattering and solar cell heating. Nevertheless, the charge transfers process plays the main role in operation of organic photovoltaic devices. It remains poorly studied because of what is at the crossroads of band theory of solids and quantum chemistry.

1.3 Outline of the work

The aim of this work is to investigate fullerene-containing samples with inorganic dopants. To achieve this goal it is necessary:

1) To obtain samples of thin fullerene films with A^2B^6 dopant group on Si, glass, glass with ITO, mica and KBr substrates. To prepare solutions of some mixtures.
2) To measure photoluminescence spectra of prepared samples and x-ray irradiated samples.
3) To analyze photoluminescence spectra in the context of substrate, dopants and amount of dopants influence.
4) To analyze the results of Scanning Electron and Atomic Force Microscopy for these samples.
5) To compare these results with quantum chemical calculations.

Chapter 1 is an Introduction

Chapter 2 contain basic theory about fullerene, photoluminescence and obtaining methods of fullerene samples.

Chapter 3 is an experimental part, which contains description of experiments, technics and results of the work.

The results of this work were published in two articles: [Elistratova M. et al (2014)], [Elistratova M. et al (2015)].

Chapter 2

2 BASIC THEORY

2.1 Main information about fullerene

Fullerene is a molecular formation from carbon atoms, which belongs to carbon allotropes class. Usually fullerene appear to be closed shape polyhedron with even numbers of atoms. Fullerene C_{60} (fig. 1.) occupies the central place among the other fullerenes. It has the highest symmetry and, as a consequence, the greatest stability.

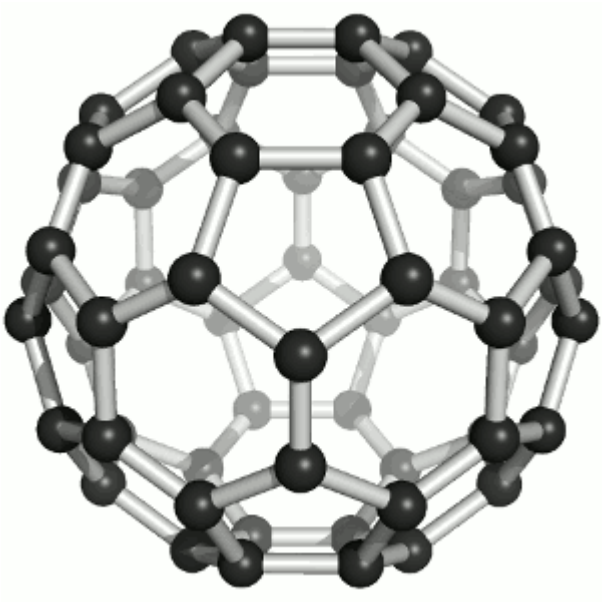

Figure 1.Molecule of fullerene C_{60}.

2.1.1 C_{60} molecule geometry

C_{60} molecule has truncated icosahedron form. This truncated icosahedron has 20 hexagons and 12 pentagons of carbon atoms. Each hexagons borders with 3 hexagons and 5 pentagons and each pentagon borders only with hexagons. Thus, every carbon atom is on the top of two hexagons and one pentagon, and all of them are similar to each other. The number of polygons in the molecule is determined by the Euler formula:

$$\sum_n N_n(6-n) = 12s, \quad (1)$$

where n is polygons dimension, N_n is the number of polygons n dimension and s is the characteristic curvature of the surface (s=1 for a sphere and s=0 for a plane). From this formula is obtained that for the spherical surface formation we need 12 pentagons (n = 5), and any number of hexagons (n = 6).

2.1.2 Solid phase of fullerene

Fullerene molecules can form molecular crystal with a face-centered cubic lattice (FCC). The solid formation of pure fullerene is called a fullerite. In such crystals, molecules form large interstices around four octahedral and eight tetrahedral gaps in the unit cell of the lattice. Actually all elements from periodic table and even some molecules can penetrate into these gaps without any disturbance for crystal structure, because the space are enough big (fig. 2). The radius of an octahedral gap is 3.06 Å. The radius of tetrahedral gap is 1.12 Å.

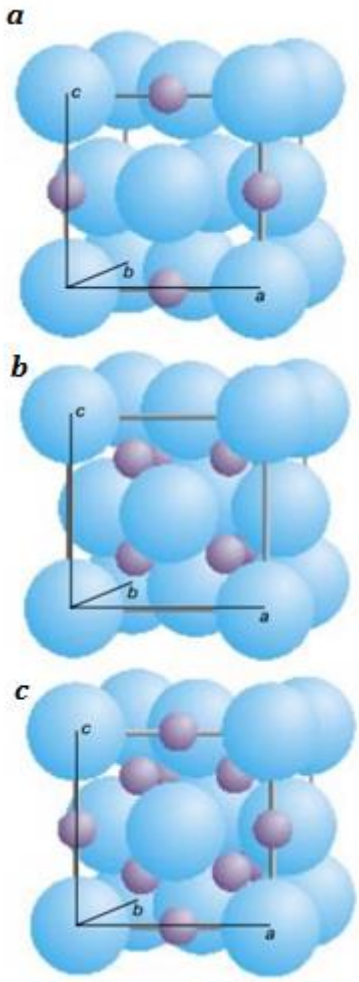

Figure 2. The voids filled in C_{60} lattice by metal atoms: an octahedral (a), a tetrahedral (b), octahedral and tetrahedral gaps (c).

Carbon atoms connect with each other by covalent bonds in a single C_{60} molecule. However, molecules in the fullerite crystal are connected by van der Waals force. Due to these facts, it is possible to dope fullerite using four different ways. Fullerite with metal atoms inside its gaps is fulleride.

2.1.3 Fullerite doping ways

1. Intercalation: doping atoms are in the fullerite crystal gaps (as in fig. 2). It can be performed by co-deposition of C_{60} and doping material in vacuum or by diffusion of doping atoms in pure fullerite crystal. Diffusion reactions can proceed spontaneously or under the influence of external factors, such as high pressure, temperature or electric field (applied to the sample).

2. Internal doping (endofullerenes): doping atoms are inside C_{60} molecule (fig. 3.1 a). Endofullerene synthesizes at the technological stage of the C_{60} molecules formation in the most of projects. It reached by placing the doping atoms if you place doping atoms gas in the vacuum quartz bulb where fullerene is obtained from graphite. Another way of endofullerenes synthesis is ion implantation with low energy [Katz at al. (2000); Katz (2001); Katz (2008)]. Thin fulleride Li@C_{60} films have been already grown. Li@C_{60} – is a fullerene with Li atom inside.

3. Doping by atomic replacement: One or more dopant atoms (not carbon) replace carbon atoms on the surface of fullerene molecule (fig. 3.1 b.). This type of doping is typical for IV group elements such as silicon and germanium.

4. Doping by addition reaction: It is possible to combine various types of big molecules, clusters or organic formation with fullerene. It was shown [Katz (2008)] that this method permits to obtain complexes with metals and various organic molecules. This method can be regarded as the fourth fullerites doping type. Fig. 3.2 shows different types of molecular structures, which are used in solar panels based on fullerenes.

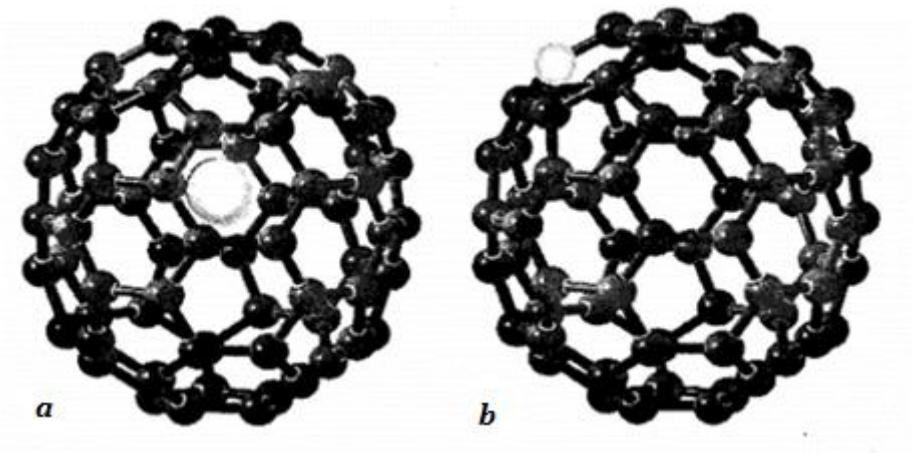

Figure 3.1. Fullerene doping: a –internal doping (endofullerene), b – Atomic replacement.

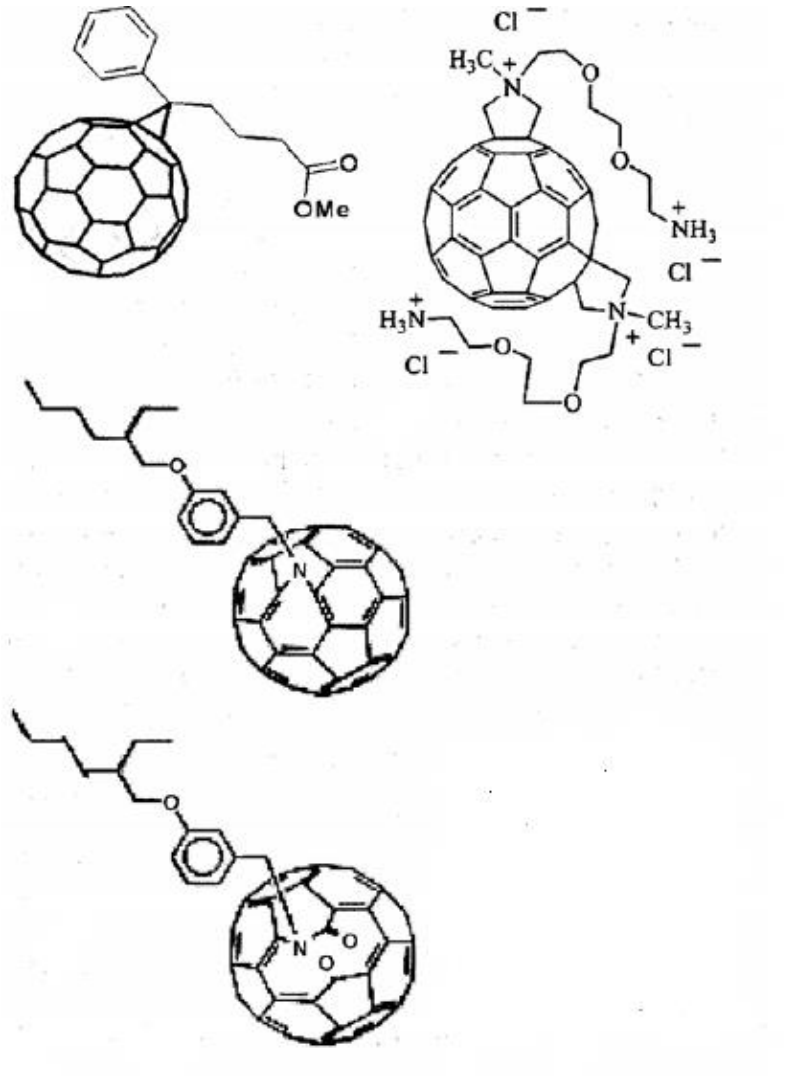

Figure 3.2. Molecular structures of C_{60} derivatives, which are used in solar cells [Katz et al. (2008)].

2.1.4 Solid C_{60} electron structure

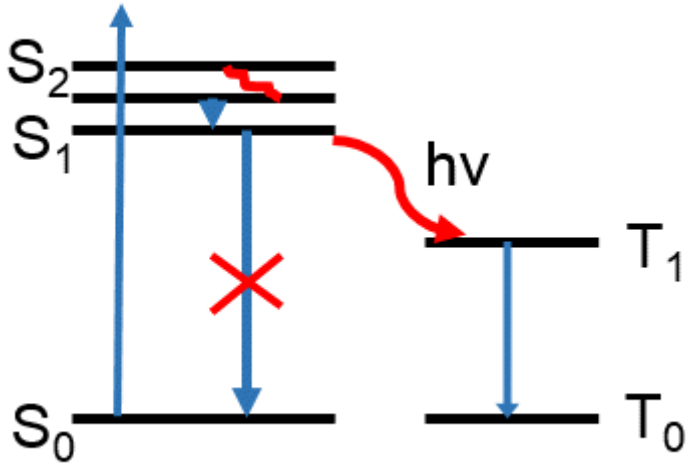

Figure 4. Solid C_{60} electron structure.

Crystalline C_{60} is a semiconductor with a band gap minimum in X point of Brillouin zone. It was mentioned above that fullerite is a molecular solid crystal. That is why it may be expected that solid C_{60} electron structure looks like electronic levels set of a single C_{60}.

Describing the fullerite it is important to remember that fullerite cannot be described as a usual semiconductor. Usual semiconductor has single atoms at the lattice sites, but fullerite has big molecular formations of 60 carbon atoms. To describe and redefine a band gap for fullerite we will use ideas of boundary orbitals: highest (by energy) occupied molecular orbital (HOMO) and lowest unoccupied molecular orbital (LUMO). HOMO and LUMO are separated from each other by an energy gap. This gap is an analogue of the band gap for a molecular crystal. However, a name “band gap” is commonly used for molecular structures by the force of habit.

C_{60} molecule is made of hexahedrons, consist of carbon atoms. Such formations have conjugated bonds. Number of π-electrons in conjugated systems of organic molecular compounds always even. That is why summary spin moment (S) may accept only integer values. When all electrons have pairs then S=0. If for one electron spin change its direction, its spin is added with the electron spin, which was not paired earlier. For this moment, summary spin moment becomes 1. Value of the spin moment S defines a multiplicity of the molecule states in general. Multiplicity is a number of ways of a total orbit and spin moments

relative orientation in the molecule. This number is determined by multiplicity index 2S+1. Therefore, states with S=0 when all electrons in a molecule have a pair are called singlet states. When S=1 multiplicity is 3 and electrons are unpaired, so this state is named triplet.

Electron structure of solid C_{60} is shown on figure 4. Singlet ground state is usually denoted as S_0, singlet excited state are S_1, S_2, ... For each excited singlet state (S1, S2, S3 etc.) there is a corresponding triplet state (T_1, T_2, T_3 etc.). Triplet state is always lower in energy than the singlet because of a Pauli principle: two electrons with the same spin cannot come close to each other. Thus, triplet state characterized by larger distance between electrons than for singlet, so electron repulsion decreases and the molecule energy becomes lower.

2.2 Photoluminescence

2.2.1 Basic information about photoluminescence

To describe electrical and optical properties (like light absorbtion process and photoluminescence (PL)) of nonconductive crystal it is usually enough to consider the highest occupied zone (HOMO or valence zone (E_v)) and lowest unoccupied zone (LUMO or conductive zone (E_c)). Energy band gap that is usually denoted between HOMO and LUMO as E_g (energy gap). Nonconductive crystals with a very big value of Eg belong to a semiconductor class.

If electron from E_v somehow went to E_c, the place where electron was before became a positive part of energy (electron vacancy). Kinetic energy of electrons $E\,{}^{e}_{k}$ and holes $E\,{}^{h}_{k}$ dependencies from momentum are defined by important equations: $E\,{}^{e}_{k} = \frac{p^2}{2m_e}$, $E\,{}^{h}_{k} = \frac{p^2}{2m_h}$, where m_e and m_h are effective masses of electron and holes. m_e and m_h are usually smaller than electron mass in vacuum m_0. Energy diagram of semiconductor crystal is shown on figure 5. Electron transition from *Ev* to *Ec* is shown by solid line. Electron appears in E_c after absorbing a light quant. It is a process of a photogeneration. The impulse saving law is valid. Minimal energy of free charge carriers is according to zone extremums. In this situation, an electron goes down to the bottom of *Ec* and a hole goes up to the roof of *Ev*. If we put more energy than electron can absorb, surplus of energy goes to increase of thermal vibration in crystalline lattice, what is in another words represents as increase of thermal particles, phonons.

Next reverse process, recombination, will be considered. Electron goes back to E_v and a hole will disappear. The energy surplus can emit as a light quant, photon. This process is called luminescence.

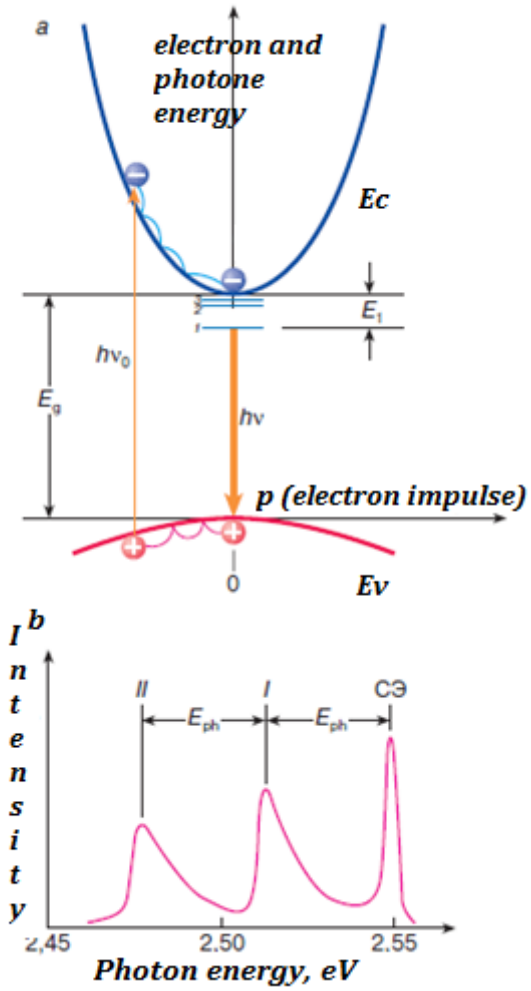

Figure 5. Photoluminescence process diagram. Generation and recombination. Spectra is shown lower part of the figure [Agekyan V. F. (2000)]

2.2.2 Exciton effects

It was found that electrons and holes have enough time to form excitons before they recombine. Excitons are bond states of electrons and holes, which can be stable because of the Coulomb attraction. It can move free through the crystal. For complete fullerene luminescence investigation is important to consider excitons effects.

Bond state energy is $E_n = \frac{2\pi^2 \mu e^4}{h^2 \varepsilon^2 n^2}$ in this situation. The lowest exciton state according to n=1. Emitting recombination of electrons and holes in excitons appears in this state. Thus, free excitons emitting line have to be visible in semiconductor PL at low temperature. Low temperature is the temperature when average heat energy lower than E_n. It means that excitons are stable in the ground state. These views are in agreement with the experimental spectra of CdS PL (see figure 5). Doping atoms may trap free excitons. This process leads to excitons formations. Photons emitting process appears then excitons recombine, electron and holes disappear at low temperature. This photon energy is $E_{hv} = E_g - E_1 - E_0$. Excitons formations are possible in molecular crystal too, but with some features. It is important to consider excitons effects for full describing of fullerene luminescence. There are two type of electron-hole excitation: singlet (without spin rotate) and triplet (without exchange interaction, are lower by energy). Optical processes in fullerene are equally depend on molecular and intramolecular excitons processes. The first processes can lead to the Frencel excitons formation (electron and hole are both on the one C_{60} molecule). The second lead to excitons with charge transfer (electron and holes are on different C_{60} molecules). Prohibited Frencel excitons levels are in the fullerene energy gap with energy of 1.55, 1.87, 2.2 eV. Permitted excitons appears at 3.6 eV [Kazaoui S. at. al. (1998)].

Charge transfer excitons energy can be estimated by thus equations:

$$E_э = I - A - 2P + C(r),$$

$$C(r) = -\frac{e^2}{r} - \Delta P(r),$$

where I - ionization potential; A - electron affinity; P - polarization energy; 2P - polarization energy of two charge which are infinitely distant from each other in the crystal, C(r) - Coulomb interaction energy; P(r) - polarization energy change when two charges approach each other at the distance r. Features that can be seen in optical fullerene spectra are results of two excitons type mixture. Some of these features were found in [Kazaovise et. al.

(1998)]. It was found that singlet electron transfer takes place at 1.84 eV, triplet electron transfer at 1.5 eV, luminescence quenching at 2.35 eV. Excitons effects may shift (by energy) with films thickness increase.

2.2.3 Luminescence, Fluorescence, Phosphorescence and Induced Emission

Many organic and nonorganic compounds are able to emit light (luminescent) in ultraviolet and visible spectra region. The essence of this phenomena is that, exited molecules emit purchase every in the form of light quant. Molecules can became exited by various ways so luminescence can occur as a result of a chemical reaction (hemiluminescence), a friction (friboluminescence), an electrical influence (electroluminescence) and an optical excitation (photoluminescence) [Guangjun T. et al. (2013)]. The most common view and well-studied type of a luminescence is a photoluminescence. It is divided to a fluorescence and a phosphorescence. It depends on the nature of the level from which the electron is gone (see fig. 6). Usually the ground molecule state is singlet (S), where by the S*→S transition (S* - first exited singlet state) is characterized by a high probability of emitting. It is the fluorescence. Contrariwise, the phosphorescence is a result of the T→S transition (T – the lowest triplet state), which is prohibited by the reason of a multiplicity. It is characterized a very small probability and a long luminescence duration.

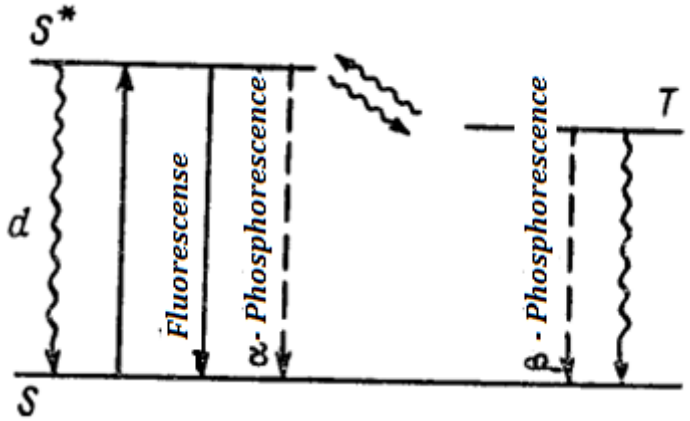

Figure 6. Singlet (S, S*) and triplet (T) levels. Transitions between them.

The main PL characteristic is the quantum yield of a luminescence (γ). This quantum yield is the ratio of emitted number of quanta per time unit to excited radiation quanta number, which is absorbed by the material in the same time. It can be shown that:

$$\gamma = \frac{Nemitted}{Nabsorbted} = \frac{f}{f+d}, \qquad (2.1)$$

where *f* and *d* are probabilities of radiation and nonradiation transitions. It follows that quantum yield change enables to take information about probability *d* if *f* is known from this formula. For example, it may be shown that quantum yield depends on excited light frequency v_{abs} in the vapor phase. There is no such dependence in solutions. The reason of this facts is that *d* is a function of vibrational energy E_{vibr} excess $(d(E_{vibr}))$. E_{vibr} excess is a result of molecule optical excitation. A molecule saves received energy until a radiation in vapor phase. It does not have enough time to collide with other molecules during 10^{-8}-10^{-9}s. Whereby $d = d(E_{vibr})=d(v_{abs})$ (see figure 7a).

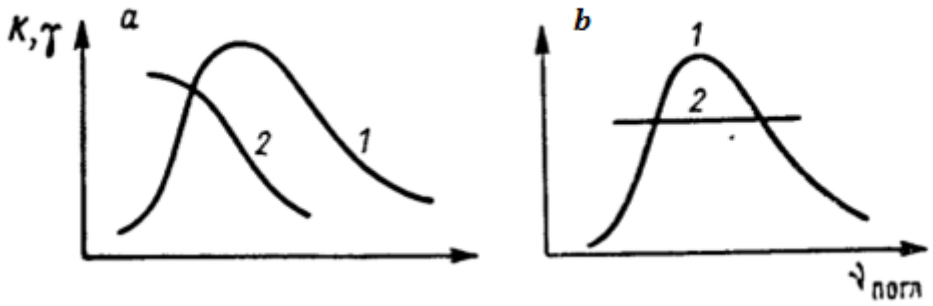

Figure 7. Absorbtion spectra (1) and quantum emitting dependence (2) of excited light frequency schematic view. For vapor phase [a] and liquid [b].

Contrariwise, excited vibrational energy is transmitted to medium very fast in liquid (see fig. 7 b). Thereby starting emission does not depend on v_{abs}, so $d \neq d(v_{abs})$.

2.2.4 Experimental results and theoretical C_{60} photoluminescence models analysis.

C_{60} photoluminescence of photo- and electroluminescence were carried out since C_{60} obtaining. Theoretical calculations of PL spectra appears as a result of computer technology development and possibility of complex quantum-chemical calculations. Complex common model was developed in [Guangjun T. (2013)]. This model based on the density matrix calculations (DFT methods, or density of functional theory). Fluorescence and phosphorescence spectral properties of C_{60} were calculated using DFT theory. Luminescence was induced by scanning tunneling microscope. These processes scheme is shown on the figure 8 a. A ground state for C_{60} is a singlet state. Transition in excited state is possible only by two processes: electron tunneling and plasmon excitation. Fluorescence and phosphorescence calculated spectra are shown on figure 8 b. Both spectra are similar. The

similarity appears because of $S_1 \rightarrow S_0$ and $T_1 \rightarrow S_0$ have similar displacement vectors. A comparison of calculations with an experimental data is shown on figure 9.

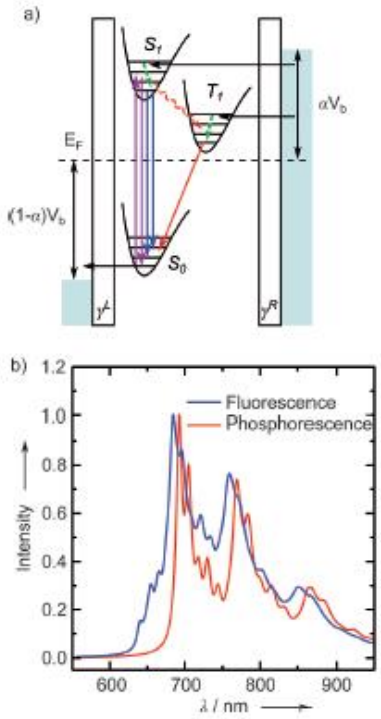

Figure 8. Possible processes of excitation and emission are indicated by arrow line (a). Nonradiative transitions are shown by dotted line. Calculated fluorescence spectra (blue) and phosphorescence (Red) (b) [V. Capozzia et al. (2001)].

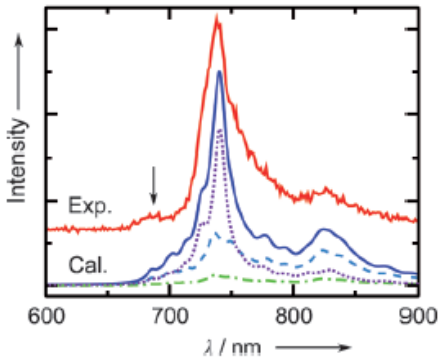

Figure 9. Measured and calculated electroluminescence spectra under the excitation of surface plasmons of C_{60} (t = 5.0 fs, hw = 2.00 eV, $E_0 = 5.0 \cdot 10^7$ Vm^{-1}, $HWHM$=100 cm^{-1}). Excited radiation - the dotted line, spontaneous excitation- dash line and electron tunneling stimulated emission - the dash-dotted line [V. Capozzia et al. (2001)].

ln [V. Capozzia et al. (2001)] basic PL spectra are interpreted by Herzberg-Teller (H-T) and Jahn-Teller (J-T) vibronic coupling of the electronic states with appropriate molecular vibrational modes. Intramolecular polaron-excitonic recombination, emissions that depends only with electron singlet and triplet transition and excitons effects are involved in this interpretation.

Three types of fullerite crystal were grown by thermal vacuum method [V. Capozzia et al. (2001)]. The first and the second types called OTT and SAT and they were grown by using a two-zone heater (95.5 cm long). Scanning electron microscopy X-ray diffraction analyses showed that these crystals have hexagonal and cubic lattice with a (111) and (110) crystallographic orientation, accordingly. The third crystal type was grown by sealed ampoule technique with a multiple sublimation procedure introduced in reference. This type called SAT-MS and it was investigated by x-ray diffractometry. The measurement showed a face cubic centred structure whose hexagonal facets are (111) oriented. A laser with the

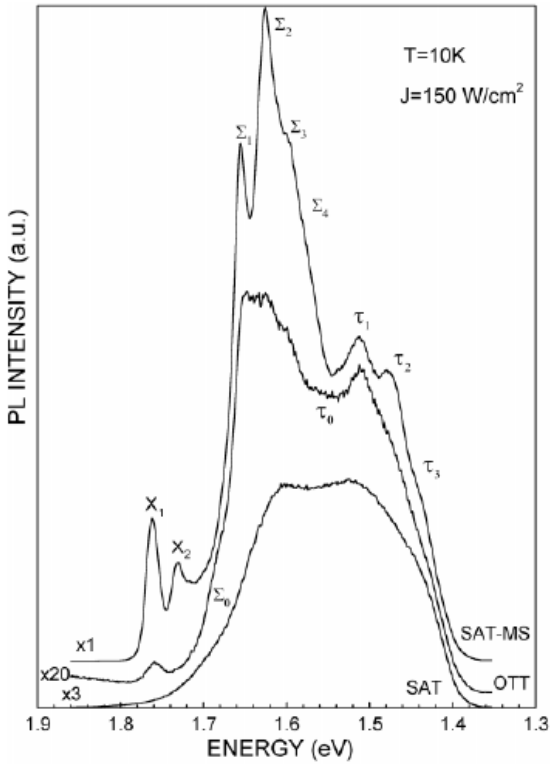

Figure 10. PL spectra of C60 SAT-MS, OTT and SAT samples measured at 10 K. The sample were photoexcited by the line 514 nm of an Ar ion laser at the intensity of 150 Wcm^{-2}. The sensitivity factor is indicated at the left hand side of each spectrum; the attribution of each PL structures is reported in the text, the spectral resolution is of 1 meV [V. Capozzi et al. (2005)].

excitation line of 514 nm was used as excitation source for PL measurements. It was focused into a 100 μm diameter beam. Measured PL spectra of all types samples are on figure 1. Structures spectral positions are similar, but resolution and intensity change for three samples. Three energy region may be observed in spectra. There are region A with the energy E > 1.72 eV, region B with 1.72 eV > E >1.55 eV and region C with E < 1.55 eV. Peaks broadening in OTT and SAT sample occurs because of a large amount of crystal defects. It depends on the deposition method. Various defects in the crystal may change the PL spectrum shape. It can be concluded that the multiply sublimation procedure before the general deposition leads to an improvement in the crystal quality, which is evident from the third spectrum. A simple diagram of the energy levels and transitions involved in the PL is shown in a figure 11.

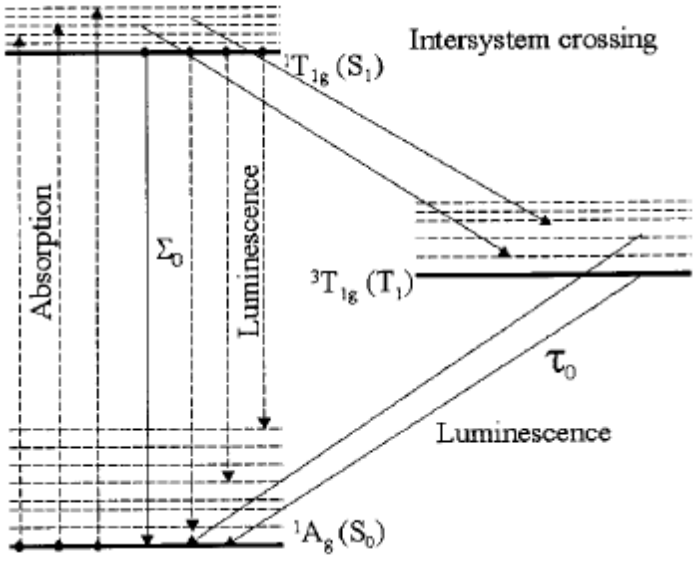

Figure 11. Energy levels diagram of transitions in C_{60} crystal. Arrows indicate the electron-vibrational transitions between the ground state and the excited state, singlet or triplet states for absorption and emission [V. Capozzi et al. (2005)].

Photoluminescence was measured at 10 K. Low temperatures lead to some features at spectra. "The features Σ_1, Σ_2, Σ_3, Σ_4 appearing as a result of vibronic transitions from the first excited singlet state S_1 to the ground state S_0 of the intramolecular polaron exciton of Frenkel type. The purely electronic transition S_1 - S_0 is a forbidden dipole transition in an ideal crystal according to symmetry selection rules. However, in a real crystal the S_1 - S_0 transitions becomes partially allowed, because lattice defects and disorder can relax the

symmetry selection rules [V. Capozzi et al.:(2001)]". Features appear as doublets (for example X_1-X_2, Σ_1-Σ_2, Σ_3-Σ_4, τ_1-τ_2) with the energy of about 0.03 eV. This fact is shown very good in SAT-MS sample. It is due to the appearance of two different crystal regions inclusive the same radiative transition. This phenomenon indicates to the differences of photoluminescence properties on molecular lattice rotational phases in fullerite. In fact, in glassy phase (the phase transition from free rotation phase to glassy phase occurs at T <90) C_{60} are frozen in two axes corresponding to two different configurations for to neighboring C_{60} molecules. Two polycrystalic domains are created. Axes remain frozen in two corresponding directions. The molecular rotations quenching does not allow switching between two possible energy configurations. This fact may explain the doublets line presence.

Molecules start to execute rotational transition between two energy states at the temperature more than 90 K. it is shown at figure 12.

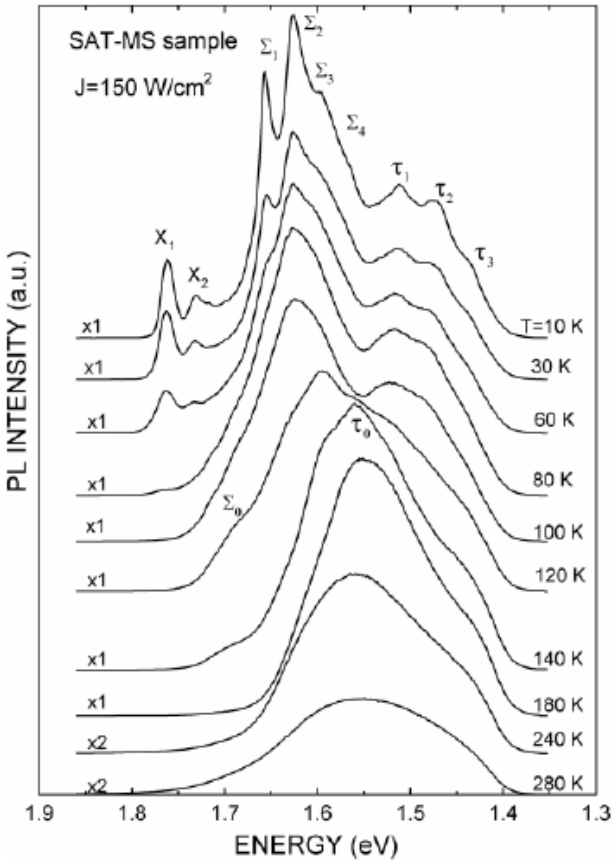

Figure 12. Photoluminescence spectra of SAT-MS crystal at various temperature [A. V. Nikolaev et al. (2008)].

Optical properties calculations were made by the density functional method in the «Theoretical study of molecular electronic excitations and optical transitions of C_{60}» work [A. V. Nikolaev et al (2008)]. Authors present their results into a table and show all features of the C_{60} energy states (see table 1)

Table 1. "Selected molecular excitations calculated with semi-empirical CI calculations and in the present work. Energies are in eV. NCSF stands for the number of configuration state functions used for CI calculation" [A. V. Nikolaev et al (2008)].

Reference	[9]		[8]	[10]	This work
Method	PPP		QCFF/π	CNDO/S	*Ab initio* SCI
N_{CSF}	134		266	900	2857
	Planar	3D			
$1\,^3T_{2g}$	2.456	2.232	2.06		2.549
$1\,^1G_u$	3.603	3.381	3.21		4.700
$1\,^1H_u$	3.635	3.391	3.15		4.771
$1\,^1T_{1u}$	4.227	4.000	4.08	3.40	5.796
$2\,^1T_{1u}$	4.750	4.681	4.53	4.06	6.335

This example shows the possibility of using the density functional method for various calculations in C_{60} investigation process.

2.3 C_{60} films obtained by vacuum deposition

2.3.1 The general laws of vacuum deposition from molecular beam

The essence of thin films depositing process is material heating in vacuum to specific temperature. In high temperature kinetic energy of atoms became enough big and they can separate from the surface and spread in the surrounding space. Own vapor pressure of the substance became bigger by several orders than the residual gas pressure also at this temperature. In this case, the atomic flux propagates in a straight line and molecules after collisions condense on it. The evaporation process is going on the usual way: a solid phase – a liquid phase – a vapor phase. Some of materials go to a vapor phase without a liquid phase (magnesium, cadmium, zinc, fullerene and others). This process is called sublimation. These conditions are provided at a residual pressure P_0=10^{-4} Pa. this vacuum can be easily achieved by using a mechanical and high-vacuum diffusion pumps connected in series. The

substrate temperature during the deposition process has a significant impact on the film structure and, consequently, the stability of its electrical properties.

The main advantages of this method are [Stijn De Vusser at all (2006)]:

- Possibility of metal, alloy, semiconductor compounds and dielectric films deposition.
- Simplicity of realization.
- High evaporation rate and the ability to control it in a wide range by varying the evaporator input power.
- This process is aseptic. In this case, high quality films can be obtained without any contaminants (in high and if it necessary ultrahigh vacuum).

Molecules evaporated in the vacuum and take in thermal energy substantially from thermal radiation [Dresden J., Frob H., (2008)]. For the most of material heat conductions has less importance when heat conduction is negligible to powder form of material. Generally, evaporated flux can be calculated by Herz-Knudcen equation:

$$\Phi_{\varepsilon} = \frac{\alpha_{\varepsilon} N_A (p_e - p_h)}{\sqrt{2\pi MRT}} = \frac{dN}{A_e dt_e} \ ,$$

where α_{ε} is evaporation coefficient from 0 to 1, p_e is a the equilibrium vapor pressure, p_h the hydrostatic pressure, M is the molar mass, R is the general gas constant, N_A is the Avogadro number and T is the temperature. The maximum evaporation intensity can be achieved when A_e=1 and p_h=0. A coefficient A_e depend on quality of deposition substrate. Clausius-Clapeyron equation can be used to approximately calculation of the equilibrium vapor pressure:

$$\frac{dp_e}{dT} = \frac{\Delta H(T)}{T \cdot \Delta V} \ ,$$

where $\Delta V = V_{vapor}$ (volume of the solid or liquid phase is negligible), the equation of the ideal gas reads:

$$\frac{dp_e}{dT} = \frac{\pi_{\varepsilon} \cdot \Delta H(T)}{RT^2} \ ,$$

For small temperature ranges the dependence of the evaporation enthalpy on the temperature can also be neglected. The result is an exponential dependence of the vapor pressure on the temperature and exponential dependence of the deposition rate on the temperature. Figure 13 shows the dependence of the deposition rate on the temperature

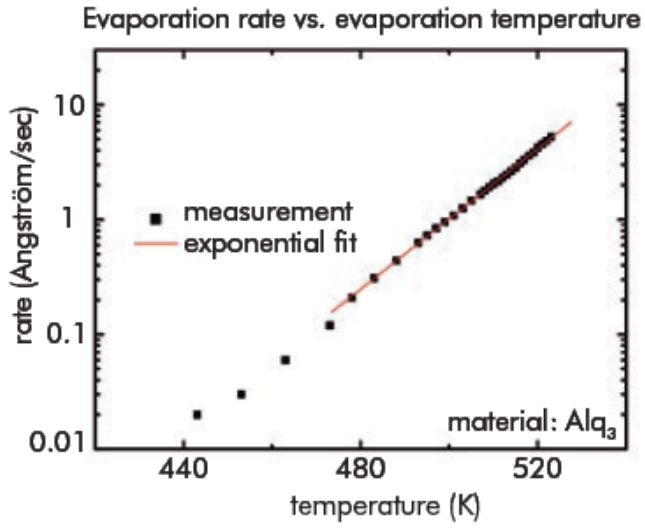

Figure 13. The dependence of the deposition rate on the temperature. The theoretical model is shown by the red line, experimental result is shown by the black line [Dresden J., Frob H., (2008)].

Furthermore, the materials thermal behavior used for the evaporation, the vapor flow distribution (characteristic of evaporation) and the layer thickness are in particular importance. Purposeful creation of homogeneous films is possible if all parameters are known in advance.

The simplest evaporator case source is a plane small-area source as shown in figure 14.

There is an angle dependence of gas flux:

$$\Phi(\varphi)=\Phi_0 \cdot \cos^n\varphi$$

where $\Phi_0=m/\pi$ is "the density of the vapor flux vertically to the evaporator plane, and m as mass per time unit to be vaporized" [Dresden J., Frob H., (2008)], Φ shows only flux emitted into the solid angle element. Films thickness depend on inclination angle of substrate. Thereby, equation for the vertically attached substrate above the evaporator cell at the distance R is:

$$\Phi_{substr}=m/P^2\pi \cdot Cos^4\varphi.$$

Evaporation geometry can be changed, however, the most common used evaporator consist not only from evaporator, but they may contain chiefly deep crucibles. The crucible wall allow to make flux more directional.

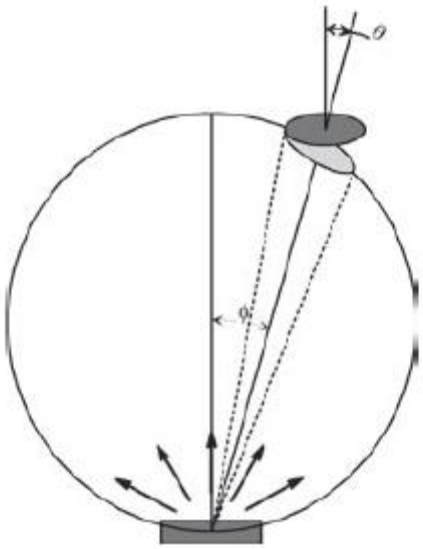

Figure 14. The simplest evaporator geometry with a point source of a Knudsen cell. Φ is an angle between the center line of a source and the position of the plane substratum element. Θ – "The inclination of the plane substratum element with respect to the center line of the source" [Dresden J., Frob H., (2008)].

2.3.2 Fullerene films growing process

The main results of C_{60} thin films deposition were prepared by deposition methods in vacuum and in helium or argon atmosphere. Microcrystalline powder sublimation at the 600 °C was used in the simplest of methods. In this method, vaporous C_{60} was condensed on the substrate. The substrate temperature can be changed irrespective of an evaporator temperature. Homogenous polycrystalline C_{60} films can be grown on substrates with low surface bond (GaAs, GaN, GeS, mica, MoS_2, Au, Ag, NaCl, KC1, KBr, LiF, WSe_2, oriented pyrolytic graphite, Be, and Sb) [Katz et all (2007)]. Another necessary condition of C_{60} growth is that the surface temperature need to be enough high to provide high C_{60} molecules mobility during the first monolayer deposition and subsequent film growth. The crystallinity degree of films increases with decreasing of C_{60} deposition rate and the substrate temperature increasing. Since the desorption temperature of C_{60} layers ranges is 230-300 °C, very sophisticated C_{60} films can be received at the temperature of 180-200 °C.

It is known that, crystalline thin film growing on substrates with weak surface bonds is possible because of high deposition rate and high substrate temperature combination. In [Katz et all (2007)] uniform thickness C_{60} films were grown with very high deposition rates

(up to 10 A / s) on a silver coated glass substrates at the substrate temperature of 300 ° C. It is turned out that the C_{60} films structure on the silver plated surface were significantly different from the structures on a clear glass. Films from clear glass substrates were almost amorphous. Films from silver plated substrates are polycrystalline with face centered cubic structures. The polycrystalline drain size was about 200 nm. The same compound films grown on mica were better than previous both types. These samples have a crystalline domain size about 500 - 1500 nm.

Moreover, the type of substrate have an effect on the films structure. Therefore, the "fullerene films" term will be used instead of "fullerite films" in further discussion. To use the "fullerite films" is not correct because fullerite is a crystal (as was mentioned in 2.1.2), but C_{60} molecules can form various types of structures. For example, polycrystalline and amorphous. On the other hand, structures with A^2B^6 doping have no additional terms.

In [Hebard A. F. et al (1995)] it was showed that big among of dangling bonds on a substrate surface led to a to a strong connection between the C_{60} film and the substrate. Films were deposited on silicon substrate and were completely amorphous. However, it is possible to grow quite perfect crystalline films with <111> texture after the dangling bonds passivation on the silicon surface. The passivation was done by hydrogen.

In [Kano S. et al (2003)] demonstrated that a fullerene film can be grown on a nickel substrate by a graphite powder evaporating. Graphite was evaporated by continuous CO_2 laser radiation in the atmosphere of argon or helium gas at a pressure of $4\ 10^3$ or $2.7 \cdot 10^4$ Pa. lines of C_{60} and C_{70} appeared in Raman spectra. These spectra were obtained in the argon flow at 200 Torr. A massspectrometry showed that the ratio of C_{60}/C_{70} is equal to 5/1. It should be mentioned that films obtained directly from graphite without any intermediate stages (synthesis and purification of C_{60}, as examples) in this method. These results suggest that a similar process can also be realized using concentrated UV light from the sun.

Moreover, it is possible to modify grown structures after deposition. Conversion methods are described in [Iwasa Y. et al (1994)]. Two metastable forms can be obtained by this method. This synthesis is performed under a high pressure. 20 mg of fullerene powder were pressed into a tablet and were placed between two titanium getter (getter – is an oxygen scavenger).

The derived sandwich structure was placed in a gold capsule and after it in a dry quartz capsule. Heating and pumping the atmosphere occur in stages. Face-centered crystals with a

lattice constant a = 13.6 Å were found at the temperature of 300-400°C and at pressure of 5 GPa. The transition to a rhombohedral structure with a hexagonal lattice with a = 9.22 Å and c = 24.6 Å parameters appeared at the same pressure, after heating to 500-800 °C.

2.3.3 Composite structures based on C_{60}

Optical properties of composite materials based on fullerene strongly depend on its elementary composition and structural properties. Therefore, there is a possibility to synthesize new composite materials with prefixed optical characteristics.

A theoretical limit of electron lithography permission restricts only by fullerene molecule size (7Å). Fullerene molecule is several order smaller than usual polymers molecules size, so fullerene is promising material for using as electron resist.

Fullerene films have good masking properties. In this case, it is possible to use fullerene films as a resist for the subsequent dry etching of semiconductors or as a doping to conventional resists [Robinson A. P. G. et al (1996)]. However, composite nanostructures based on C_{60} obtaining techniques are rarely mentioned in articles.

Samples with gradient and different composition were obtained in the article "Optical spectroscopy of thin C_{60}:CdS composite films" [Zakharova I. et al (2013)]. There the samples were obtained by the thermal evaporation of a C_{60}:CdS mixture containing different components proportions. The films were deposed in quasi-closed volume (QCV). "The QCV method differs from deposition via a molecular beam in that the process of condensation and reevaporation near the substrate occurs in quasi-equilibrium conditions, upon strong interaction of the vapors of the substance to be deposited with the crystallites formed on the substrate surface. Such a process results in the formation of films with a high degree of crystallinity and with a small thickness without puncturing. Among the advantages of the QCV method are the high degree of homogeneity of the films fabricated in one evaporation cycle, good reproducibility of the properties of samples produced in different evaporation cycles under identical technological conditions, and the high growth rate (up to 100 nm/min), which allows one to reduce the requirements on the residual gas pressure. [Zakharova I. et al (2013)]". (QCV is a type of evaporator where substrates and mixture are placed together in one volume. A scheme and other details will be mentioned later in the second chapter.). Glass with ITO, silicon and KBr were used as substrates. The same saturation gas pressure of C_{60} and CdS is provided at different temperatures. For CdS this temperature is 100 °C higher than for fullerene. Thus, the deposition rate of CdS from C_{60}:CdS mixture is much

higher than for C_{60} at constant temperature of evaporator. For example, CdS evaporation is very slow in 700 °C, but very intensive for C_{60}. Therefore, it is possible to produce samples with different composition, including samples with a composition gradient throughout the film thickness.

All structures obtained from new materials need to be investigated by various test technique. Samples were studied by atomic-force microscopy, Raman and optical spectroscopy in this work.

Normalized spectra of fullerene film with various compounds of CdS are shown in figure 15.

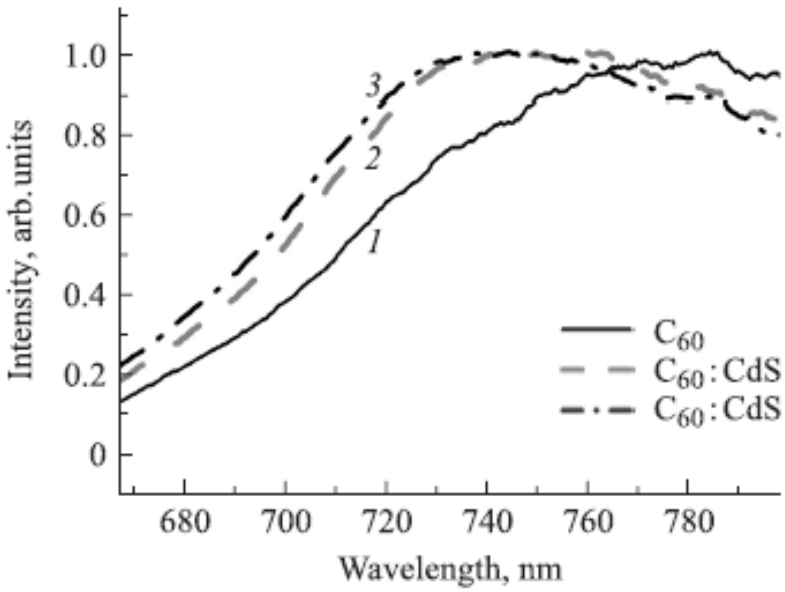

Figure 15. Photoluminescence spectra of pure fullerene (1) and samples with different proportions of CdS (2, 3). (2) corresponds to the 5:1 ratio between the components in the mixture. (3) - is 2:1.[Zakharova I. et al (2013)].

The pure fullerene peak maximum is at 785 nm. The second peak appear at 730–740 nm after CdS addition. The position of the second peaks depend on the CdS content. The peak shift is due to the changing of electron structures after forming a molecular complex with CdS.

For the future analysis of CdTe doping influence on fullerene photoluminescence, it is important to study separately luminescence properties of CdTe. It is shown photoluminescence spectra of 4.5 nm CdTe quantum dots on figure 16 [L. Pan. et al (2007)].

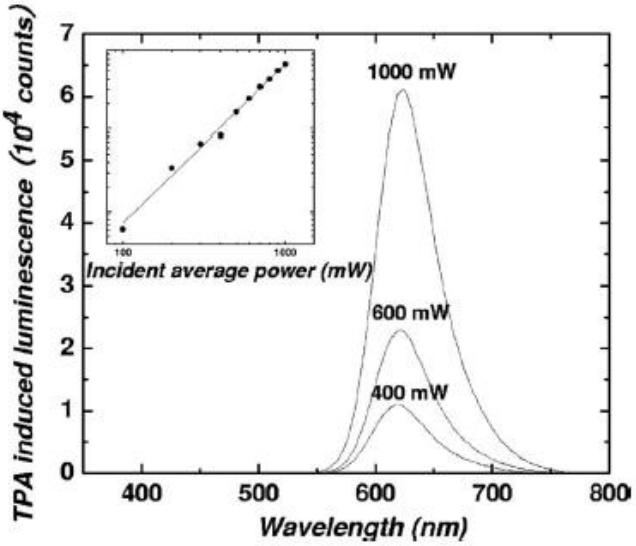

Figure 16. Photoluminescence spectra of 4.5 nm CdTe quantum dots. Three curves at variant power of laser excitation [L. Pan. et al (2007)].

Here the 630 nm peaks are visible. Nevertheless, such CdTe radiation is possible only if we have a quantum dots with equal size. CdTe has 1.49 eV energy gap, in this case, radiation of bulk CdTe is possible about 830 nm.

Composite material based on fullerene can be obtain not only by vacuum deposition but also by concretion from liquids (a coating method, a Langmuir–Blodgett method). This kind of materials find an application for photodiode and light-emitting diode production. They are suitable for photocatalysis and fluorescent mark in medicine.

The example of these material investigation is called "Well-Organized CdS/C_{60} in Block Copolymer Micellar Cores // Macromolecular Rapid Communications" [H. Koh et al (2009)]. Micellar core were obtained by solvating a a polystyrene-block-poly(2-vinylpyridine) block copolymer in polystyrene-selective toluene. Dispersing of a C_{60}-toluene solution in the CdS micelle solution with stirring led to the well-defined organization of two type of nanoparticles. They are shown on figure 17. Photoluminescence spectra are demonstrated on figure 18. There is only luminescence from singlet CdS excitation. PL of C_{60} are not observed.

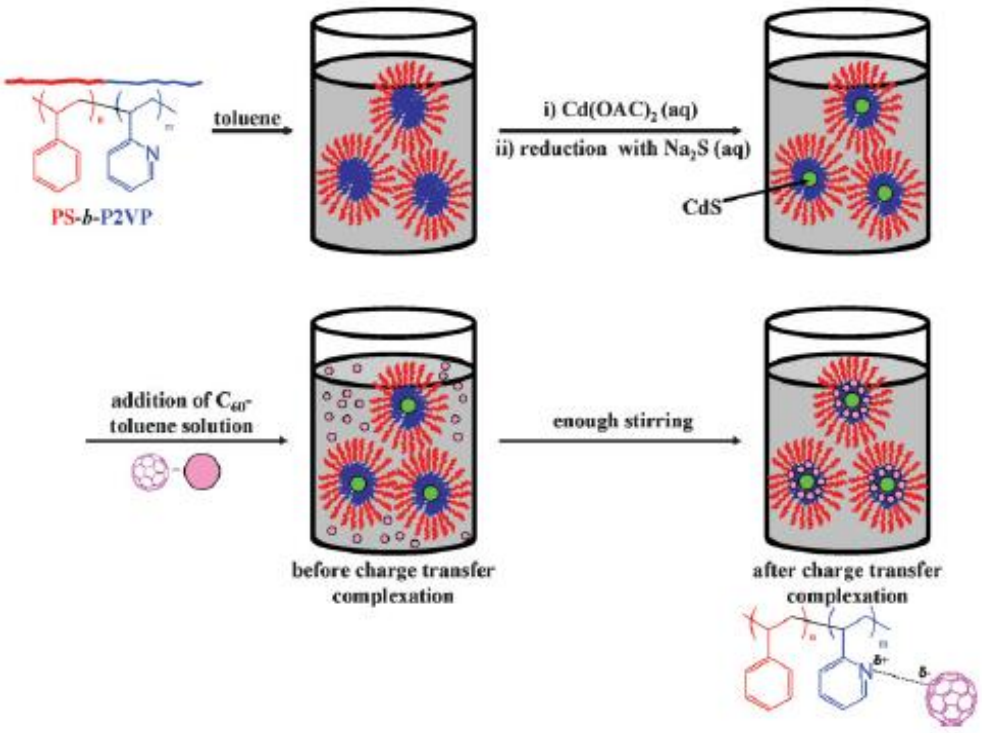

Figure 17. Synthesis scheme of well-organized CdS/C_{60} nanoparticles [H. Koh et al (2009)].

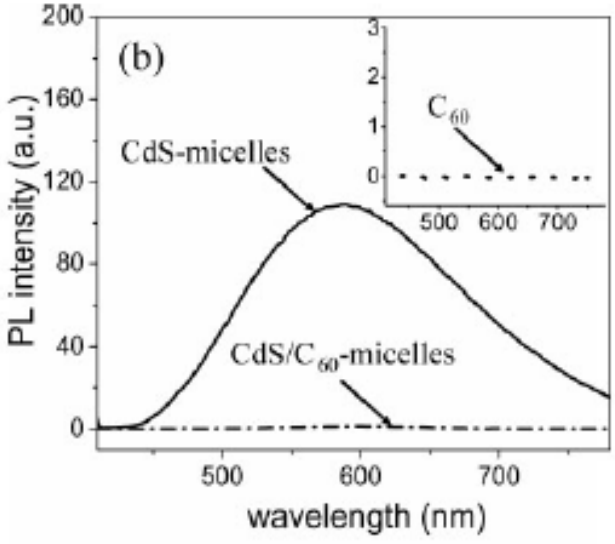

Figure 18. Photoluminescence spectra of well-organized CdS/C_{60} nanoparticles. Solid line is CdS micelles spectra, dash-dot line is a CdS/C_{60} structure, dot line is only C_{60}. [H. Koh et al (2009)].

2.3.4 Photoelectric devises with fullerene based materials

Due to the big size of fullerene molecule the film are enough spongious. It is shown on figure 19. Such spongious films may be used to obtain new form of heterojunction, bulk heterojunction (BHj) [Dennel G. et al 2009]. BHj is nonplanar version of usual Hj (see figure 20) It has higher absorption coefficient than planar Hj because of bigger junction area [Hoppe H et al. (2009)].

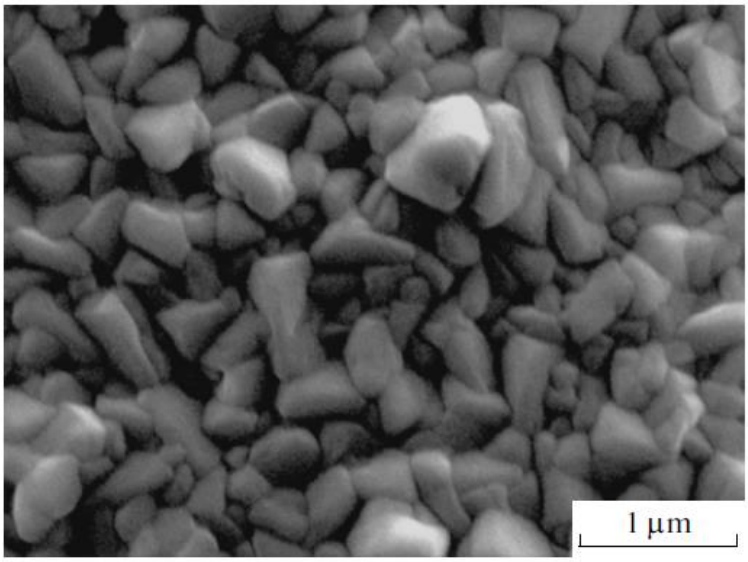

Figure 19. Surface topography of the fullerene film, obtained by scanning electron microscopy.

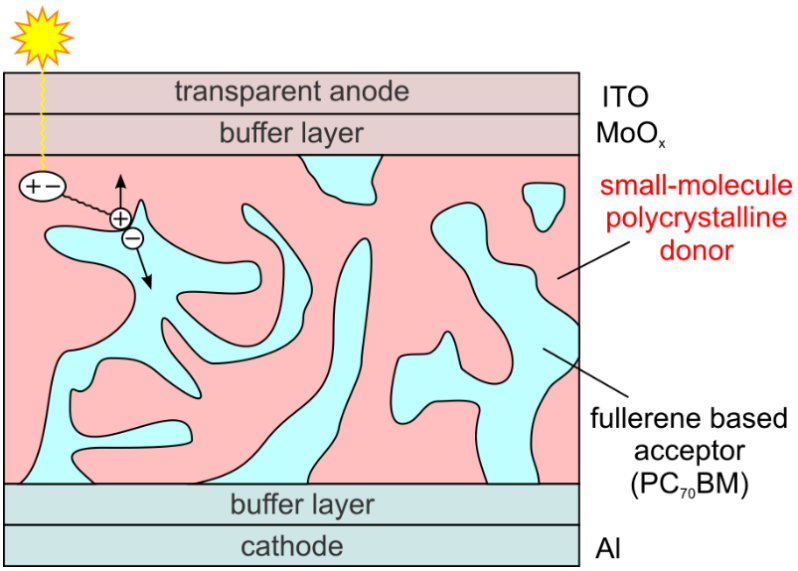

Figure 20. A solar cell based on bulk heterojunction. [Zhugayevych A et al (2012)]

It could be supposed that electron-hole pair separation occurs with higher effectivity in BHj.

Hj and BHj were compared in [Takeda A. et al (2009)]. Two mentioned structures were produced. As a result of numerous research [Lee K. J. et al (2007)] it was shown that BHj has higher coefficient of efficiency than Hj [Scharber, M. C. et al (2006)].

2.4 X-ray radiation influence on C_{60}

Developments of fullerene films and devices based on fullerene production technology in a large scale demands special studies of the behavior of fullerene-containing materials in the field. A fact about the dimerization and polymerization of fullerene under the action of light is well-known [A. Zauco et al (2005)] [K Lesper et al (2005)] [G. L Gutsev (2011)]. Polimerisation is a process of long chains of interconnected fullerene molecules formation under the influence of light. Chain consists of respectively two C_{60} molecules in the process of dimerization. Photopolymerization often occurs by the cycloaddition mechanism, when double bonds are broken and four-carbon ring is formed outside the fullerene. $C_{120}O$ dimers can be formed if films contain oxygen under the influence of light. Moreover, it is possible to obtain more compound structures under the influence of temperature and pressure. Nevertheless, optical physical and chemical properties change because of polymerization.

The radiation chemistry aspects and interaction mechanisms of fullerene with ionize radiation (x-ray and electrons) are described in [H. Klesper et al (2005)]. It was found that the most part of the X-rays is transmitted by the C_{60} films (more than 99%) and hits the underlying substrate (Si, Cr, Cu, Ag, Au, Pb, KBr, quartz). The secondary photons and electrons initiating from these processes are backscattered to a significant space into the fullerene films (see figure 21). Interest moment of this work is a result of synchrotron radiation influence on C_{60} investigations. It was found that amorphous carbon “cracks” appears under the influence of radiation and images distort. It happens when fullerene mask contains oxygen impurity (figure 22).

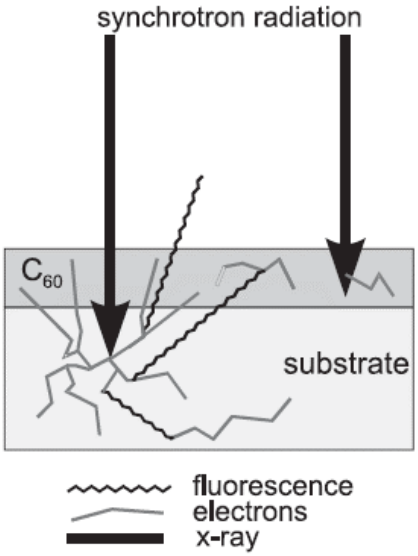

Figure 21. Schematic sketch of primary (photo-effect) and secondary (fluorescence, Auger electrons) effects resulting from X-ray irradiation of a resist-coated substrate in [H. Klesper et al (2005)].

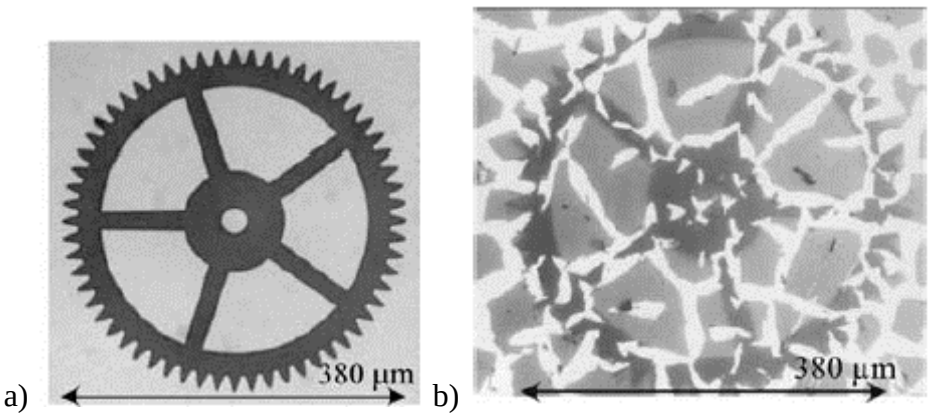

Figure 22. Carbon microstructures on a Si substrate with a fullerene mask obtained by synchrotron irradiation: Oxygen-free C_{60} films (a) and oxygen-containing C_{60} films (b). [H. Klesper et al (2005)]

It is interesting that fullerene has a negative resist behavior what it is used in x-ray lithography.

Chapter 2

3 EXPERIMENTAL PART

3.1 Experiment methods

3.1.1 Preparation methods of thin films based on fullerene

The essence of a thin films deposition process implies that materials are heated up to special temperature. At this temperature atomic and molecular kinetic energy becomes enough to separate atoms and molecules from the bulk material surface to surround space. This process becomes possible at such heating temperature when materials own vapor pressure exceed, by several order, residual gas pressure. In this case, the atomic stream propagates linearly. Evaporated atoms and molecules have collisions with the surface and then condense on it. Fullerene and A^2B^6 materials were transferred into vapor without liquid phase. Thus, evaporation is carried out in short way: the solid phase to the vapor phase. It is called sublimation. Following conditions were provided at a residual pressure of 10^{-6} Pa. This vacuum was easily achieved by mechanical foreline and high vacuum diffusion pumps. The substrate temperature has a great impact on films structure and also on its electrophysical and optical properties. In this work, substrates were kept at room temperature during the process. Sputtering on a cold substrate lead to amorphous and polycrystalline structure formation and possibly alignment on randomly distributed semiconductor clusters or molecules. The main advantage of this method is sterility of process. It allows to propagate high films quality without any contamination and what is more important without oxygen subject.

Thin fullerene films doped with CdTe and CdS were prepared by co-deposition technique from Knudsen cell and in quasi-closed volume. The schemes of evaporators is on figure 23. Open source evaporating (Knudsen cell) allows to obtain composite films on various substrates. Powder of clear C_{60} and C_{60} with adding A_2B_6 impurities was evaporated at 500-650 °C on Si, glass with ITO, KBr and mica substrate. Silicone substrates were cleaned by isopropyl alcohol. The cell was made from wolfram and surrounded by the wolfram capsule. The out part is connected to 0-1.5 V. Evaporation was produced on a pre-heated in a height vacuum up to 150°C in both methods. Then substrates were cooled to 40°C.To provide uniformly mixture distribution evaporator was slowly heated during 10 min. It promotes

better oxygen adhesion, which penetrates into fullerene. Films thickness was 200-500 nm. In comparison with the initial charge, it can lead to a significant changing of a film composition. Obtaining a large area film possibility is an advantage of the Knudsen cell. Evaporating regimes, other parameters and examples of obtained samples are presented in table 2.

a) b)

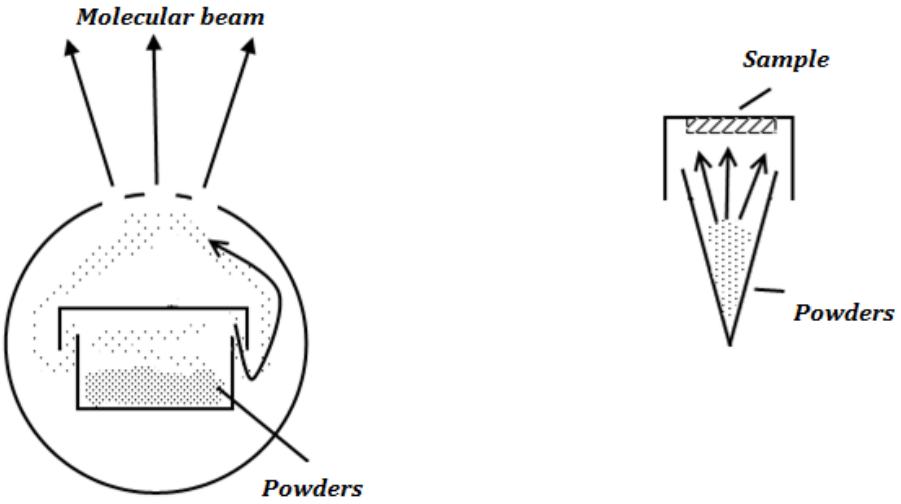

Figure 23. The schemes of evaporators. The Knudsen cell (a) and Quasi-closed volume cell (b).

Table 2. A list of obtained samples.

N	Substrate types	Mixture composition, mg	Evaporator type	T heating, *C	T substrate, *C	Film thickness, nm
230	Si, glass ITO, Mica	C60 -10, CdS -10	opensourse	150	40	120
231	ITO, Si, Mica, KBr	CdS-20	opensourse	150	40	
232	Si, ITO, Mica, KBr	C60 - 20, CdS - 20	opensourse	without control	without control	150
233	Si, ITO	C60 - 20, CdS - 20	opensourse	without control	without control	125
234	Si, ITO, Mica, KBr	C60 - 25, CdS - 25	opensourse	without control	without control	350-370
235	Si, Mi ca	C60 - 35, CdS - 35	opensourse	without control	without control	
236	Mica	C60-5, CdS-5	QCV	without control	without control	
237	Si	C60 - 5, CdTe - 5	QCV	without control	without control	
238	Si	C60 -4,5, CdS - 4,5	QCV	without control	without control	
239	Si	C60-5, CdS-5	QCV	without control	without control	
240	Si	C60-10	opensourse	without control	without control	150
241	Si	C60-10	opensourse	without control	without control	
241	Si (241)	CdS-10	opensourse	without control	without control	
242	ITO, Si, KBr	C60 - 10,CdS-10,CdTe-10	opensourse	140	40	163
243	Si	C60 -10, CdTe - 5	opensourse	130	30	
244	Si	C60 -10, CdTe - 2,5	opensourse	120	20	150
245	Si	C60 -5, CdTe -10	opensourse	120	35	125
246	Si, Kbr, Mica	C60 -10, CdTe -10	opensourse	without control	without control	
247	Si, Kbr, ITO	C60-10, CdTe -10	opensourse	230	35	
248	Si, Mica, KBr, ITO	C60-10, CdTe -10	opensourse	140-150	40	125
249	Si, ITO	C60 -10, CdTe - 20	opensourse	150	30-40	169
250	Si, glass	C60 - 20, CdS - 20	opensourse	170	30	260
251	Si, glass	C60 - 20, CdS - 40	opensourse			265
252	Si, glass, ITO	C60 - 20, CdS 60	opensourse			
253	Si (RGB)	C60-60	opensourse			
254	Si (RGB)	C60 - 60, CdS 60	opensourse			
255	Si, ITO, Mica	C60 - 30, CdTe 60	opensourse			
256	Si, ITO, Mica	C60 - 30, CdTe 60, CdS 30	opensourse			
257	Si, ITO, Mica	C60 - 45, CdTe 45	opensourse			
258	KBr, Mica, ITO	C60 - 45, CdTe 45	opensourse			
259	KBr, Si, Mica, ITO	C60-90	opensourse			
260	Mica, Si	C60 - 8, CdTe 4	QCV			
261	Mica, Si, KBr,glass	C60 - 45, CdTe 45	opensourse			
262	Si, Kbr, Mica	C60+C70- 35, CdTe - 35	opensourse			

3.1.2 Photoluminescence spectra measuring technique

Photoluminescence spectra were obtained by two type of installation: with pulsed and with continuous lasers. First type of spectra were obtained with automated installation based on monochromator MDR-2 and secondary emission photocell FEU-79. The scheme is on figure 24. Pulsed nitrogen laser AIL-3 with 337 nm wavelength and power of 3 mW produced excitation of photoluminescence. Pulse length were 10 ns with a frequency of 100 Hz. A pin-diode was used for synchronization. A quartz glass slivered a small part of light and directed it to the pin-diode. Main part of light was directed to a sample. Luminescent light was focused on input monochromator slit by a lens system. White glass filters were installed before the monochromator slit to avoid the scattering laser radiation falling into the monochromator. Output light from monochromator fell into secondary emission photocell and there it was converted into an electric signal.

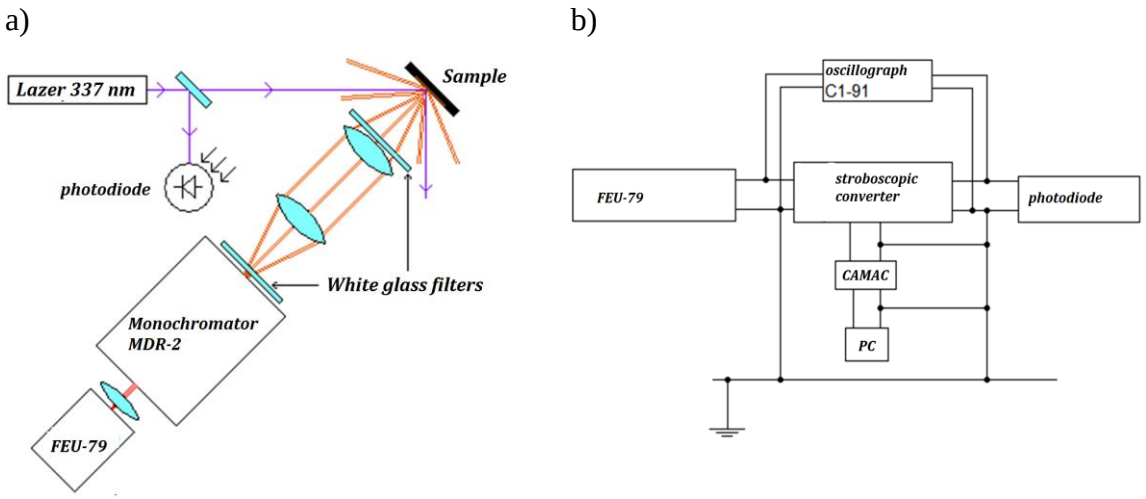

Figure 24. Optical (a) and electrical (b) scheme of installation for photoluminescence measurements.

This signal was fed to the input of stroboscopic voltage converter B9-5 with strobe pulse width of 4 ns. The signal from pin-photodiode fell to the synchronize input of the B9-5. B9-5 allows setting a delay between the arrival signal from the pin-photodiode (the maximum of the laser pulse) and the time of recording signal from the secondary emission photocell. Thus, it is possible to measure as "fast photoluminescence" spectra (in the maximum of laser pulse), as quasistationary PL (delay time not less than 1 ms). The recorded in B9-5 signal, was converted to a digital by interface device CAMAC, arrived at the peripheral board of a personal computer, and processed by the program. The resulting spectra were normalized to the sensitivity of the measuring device.

Second type of photoluminescence spectra were measured by using automated installation based on Horiba Jobin Yvon monochromator. It is composed of FHR 640 monochromator with a grating of 1200 mm-1 and the Symphony II (1024 * 256) Cryogenic Open - Electrode CCD detector. Continuous semiconductor laser with 408 nm wavelength, 50 mW powerty produced excitation of photoluminescence (laser spectra is on figure 25). Yellow glass filter was installed before the slit of the monochromator to avoid scattering laser radiation falling into the monochromator. CCD chamber was maintained at the temperature of 77 K. The scheme of installation is on figure 26.

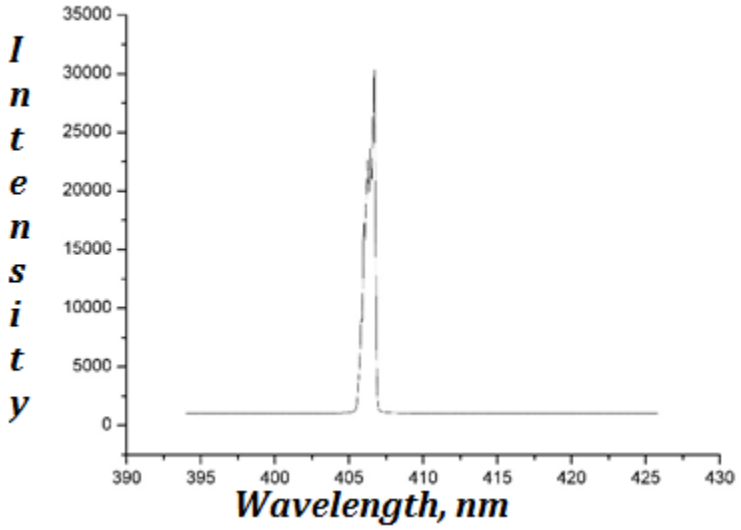

Figure 25. Continuous laser spectrum.

a) b)

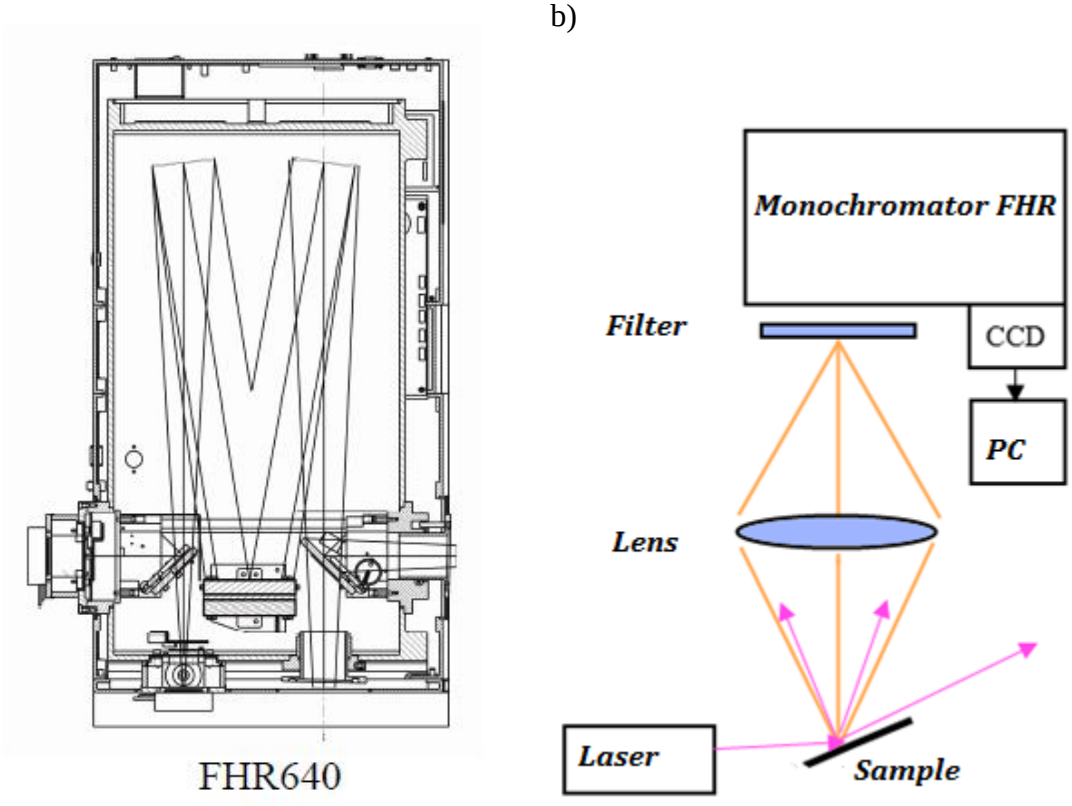

Figure 26. Figure 21. Schemes of monochromator FHR-640 (a) and installation for photoluminescence measurements (b).

3.2 Experimental results

3.2.1 Scanning electron microscopy

A scanning electron microscope Jeol JSM-6390 was used to study the surfaces morphology. It worked with resolution of 3 nm. The films' composition in the selected area was measured by energy dispersive micro-analysis console "Oxford INCA Energy" with the utmost sensitivity 0.1wt%. Figure 24 presents surface topography of C_{60}-CdTe sample containing 50% of impurity obtained by SEM. At most surface is clear without inhomogeneities (spectra 2 and 4). It may contain microcrystalline structure (spectra 1 and 3). X-ray analysis displays that these microcrystals are from C_{60}-CdTe mixture and do not contain CdTe nanoparticle.

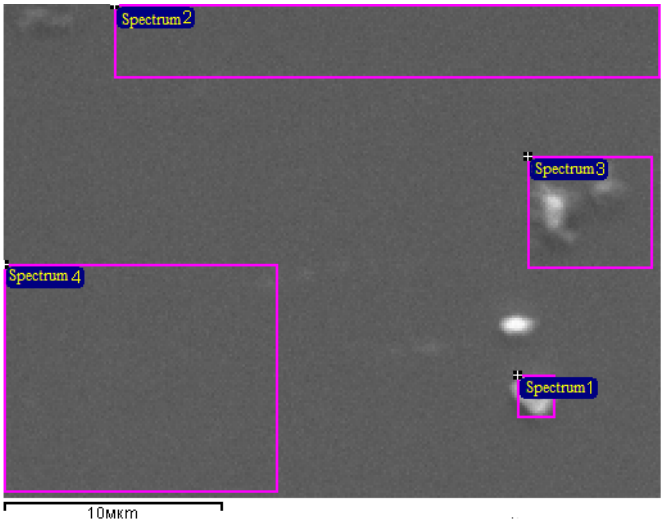

Figure 27. SEM image of C_{60}-CdTe (with 50% of CdTe) sample.

Chemical compositions spectra were measured by an energy dispersive console (table 3). All spectra contain both C_{60} and CdTe peaks. Points (2, 4) on a smooth homogeneous surface show sufficiently good uniformity of composition with an average value of Cd content of 2.37 and Te of 5.53%. At opposite to atomic masses of Cd and Te, it means that CdTe included in film in molecular form. Quantum-chemical calculations verified this fact. Silicon appeared in the spectra because the absorption of electrons and output of x-ray radiation is possible from the substrate when the film has thin thickness (about 500 nm). Oxygen also presents in spectra, because fullerene is susceptible of oxygen and water vapor. In comparison with the initial charge, which was 50% to 50%, it is noticed that amount of impurities became lower. Open source method production leads to significant depletion of the impurities in films.

Table 3. X-ray analysis result for sample containing 50% of CdTe impurities.

Spectrum	C	Si	Cd	Te	O	Total
Spectrum 1	14.32	17.84	2.35	5.34	60.15	100.0
Spectrum 2	15.47	15.69	2.33	5.68	60.83	100.0
Spectrum 3	16.39	14.06	2.33	5.53	61.57	100.0
Spectrum 4	15.43	15.73	2.48	5.59	60.77	100.0

At most all spectrum represent CdTe compound with Cd and Te average content of 2.37 and 5.53 accordingly. At the same time atomic mass of Cd and Te are 112 and 127 accordingly. Due to the simple math ($\frac{2.37}{5.53} = 0.5 \quad \frac{M_{Cd}}{M_{Te}} = \frac{112}{127} = 0.88$), it may be concluded that CdTe is in film partly in molecular form and partly films contain atomic Te.

To contrast it is shown sample № 248 with inhomogeneities (see figure 25). Through case studies of a sample of 248, it is clear that there is a three-point of scatter in composition (Table 4). In particular, visible inclusions contain a large percentage of CdTe. On a clean surface (spectrum 1) observed only carbon adsorbed oxygen, silicon - from the thinness of the film.

It is possible to find inhomogeneity contains only carbon. It is a random particle from initial mixture. It appears if evaporating rate is very fact.

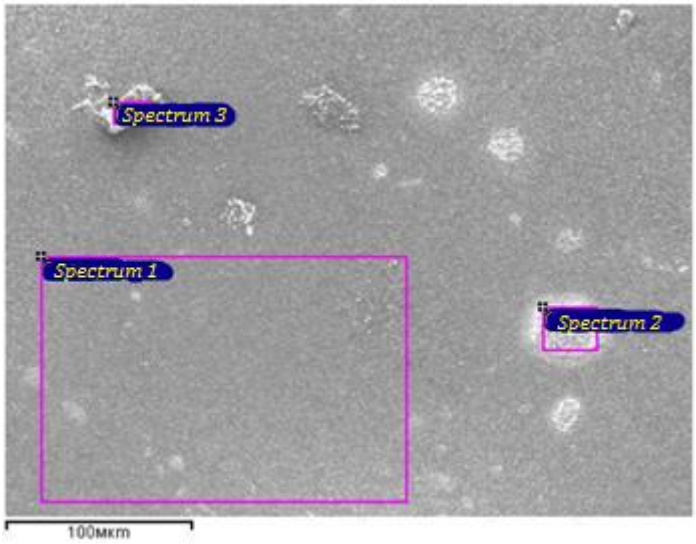

Figure 28. SEM image of sample №248.

Table 4. X-ray analysis result for sample № 248.

Spectra	C	O	Na	Si	Cl	K	Cd	Te	Pb	Total
Spectrum 1	78.40	0,63		12,78			3,66	4,54		100,00
Spectrum 2	78.00	1,46	0,69	3,43	1,14	1,18	3,73	8,16	2,21	100,00
Spectrum 3	74,02	1,73	0,31	3,19		0,65	9,33	10,78		100,00

X-ray analysis results for some samples were recalculated into molar percents without silicone part. It is shown in table 5. Data from this table give information about how the mixture was transferred to films during the evaporation process. There only sample № 237 was made by QCV evaporating and in contain all amount of initial mixture. Other samples were made by open source method and it led to significant depletion of the impurities in films, until complete disappearance of impurity.

Table 5. X-ray analysis results for samples contain various % of CdTe impurities.

№	Initial mixture of C_{60}:CdTe weight	Weight % CdTe	Molar % CdTe
242	1:1	12%	29%
243	2:1	5-7%	13-18%
244	4:1	3,5%	10
245	1:2	27%	52%
220	1:0	0%	0%
225	1:0	0%	0%
228	10:1	Not found	Not found
237	1:1	50%	74%

The same measurements were done to C_{60}-CdS containing films. The results has some differences much smaller amount of CdS: transferred to films from initial mixture. It appears because the saturated vapor pressure of CdS is significantly lower than for C_{60}, thus, evaporation occurs under nonequilibrium conditions. The saturated vapor pressure of CdTe and C_{60} are particularly equal. Therefore, CdTe transfers better into films.

3.2.2 Atomic force microscopy

Atomic force microscopy was used to study surface morphology with a view to find C_{60}-A^2B^6 interface and to estimate films quality. Figure 26 shows 3-dimentional images of fullerene films with CdTe and CdS doppings.

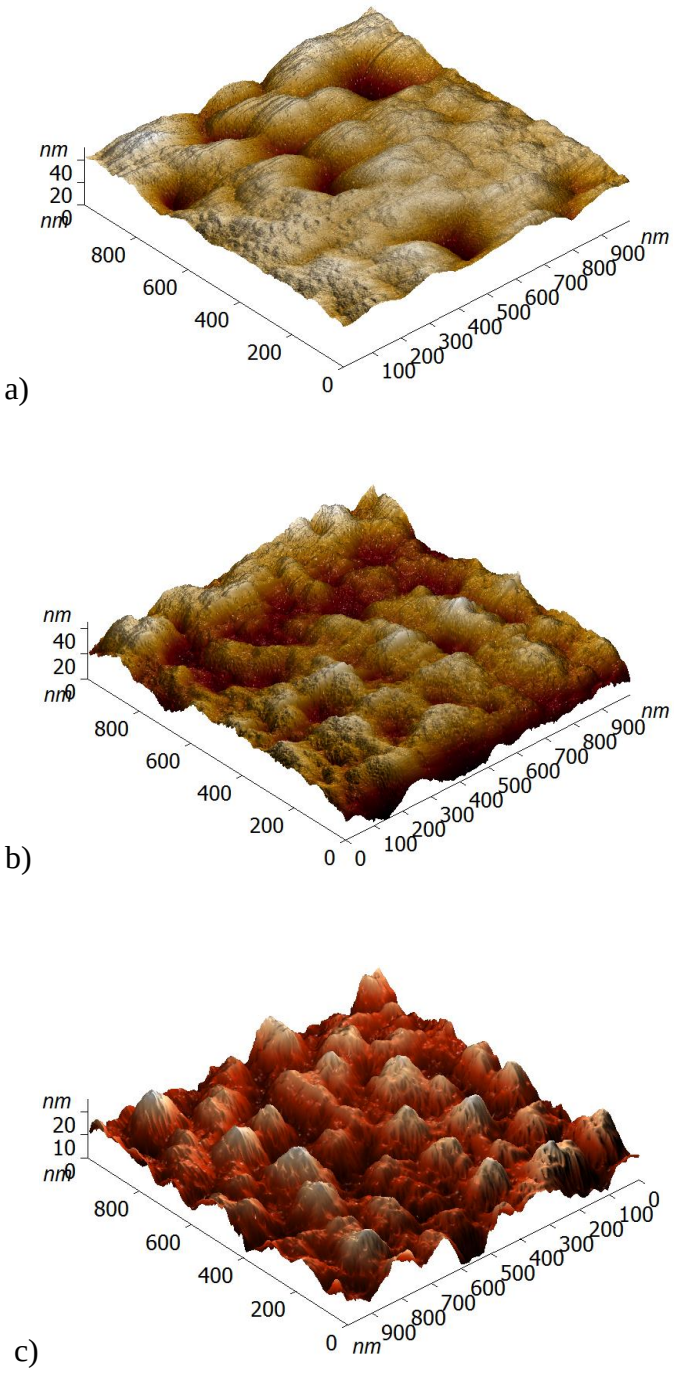

Figure 29. 3D AFM surface image of the C_{60} film (a), C_{60}-CdS (b) and C_{60}-CdTe (c)

The surfaces have a clear-cut hilly relief typical for vacuum-deposited fullerene films [Pakhomov D. L. et al. (2012)], [Li L et al. (2008)]. It is most likely that hills are crystalline or polycrystalline formations, "since their faceting and/or preferred direction (inclination) relative to the substrate are unclear" [Pakhomov D. L. et al. (2012)]. There the C_{60}-doping interfaces are not observed. Clear C_{60} and C_{60}-CdS are similar because only small amount of CdS penetrate into C_{60} matrix. There is the difference in the topologies of the C_{60} and C_{60}-CdTe films is noticeable: crystalline hills of C_{60}-CdTe (c) are sharper and amount of hills is bigger It may occurs due to the molecular complexes formations, but to confirm this supposition the quantum-chemical calculation need to be done.

3.2.3 Photoluminescence measurements

The analysis of previous investigation shows that two peaks at wavelength of 720-730 nm (1.72–1.70 eV) and 800-820 nm (1.55 – 1.51eV) appear at photoluminescence spectra of pristine fullerene. The second peak (820 nm) is associated with the radiation from the vibrational sublevels, and the first one is associated with a $T_1 \rightarrow S_0$ transition, which must be enough slow. The difference in the experiment between the two maxima corresponds to the energy of the phonon modes of the C60: the difference between the peaks is about 200-150 meV, which corresponds to the fundamental vibrational modes of fullerene (1200-1600 cm^{-1}). The graphs are shown in Figure 27 and 28. Transitions about 1.5-1.6 eV correspond to $S_1 \rightarrow S_0$ transitions.

Pristine fullerene films has wide PL peak with about 725 nm maximum (figure 27, black line). The large peak width explained by two fullerene peaks contribution - at 720 nm and its vibration recurrence at 830 nm. Impurity adding leads to extra peaks appearing at the wavelength of 630 nm. This wavelength accords to the energy of singlet-singlet transition in C_{60} energy structure. Such transition is forbidden for an isolated fullerene molecule for the reason of symmetry, but if impurity forms a molecular complex with C_{60}, symmetry of the cluster is reduced (from T_h to C_s). "The extra peak intensity increases with amount of impurity due to the increasing amount of molecular complexes formation. The sample with 50% of CdTe (figure 28, black line and sample 237 from table 2) shows main peak at 630 nm wavelength. It may be associated with overwhelming contribution of singlet-singlet transition in luminescence. According to the results of quantum-chemical calculations (will be presented further in the work), in case of optimization geometry, CdTe molecular is located on 6-6 bond of fullerene. "[Elistratova M. et al (2014)].

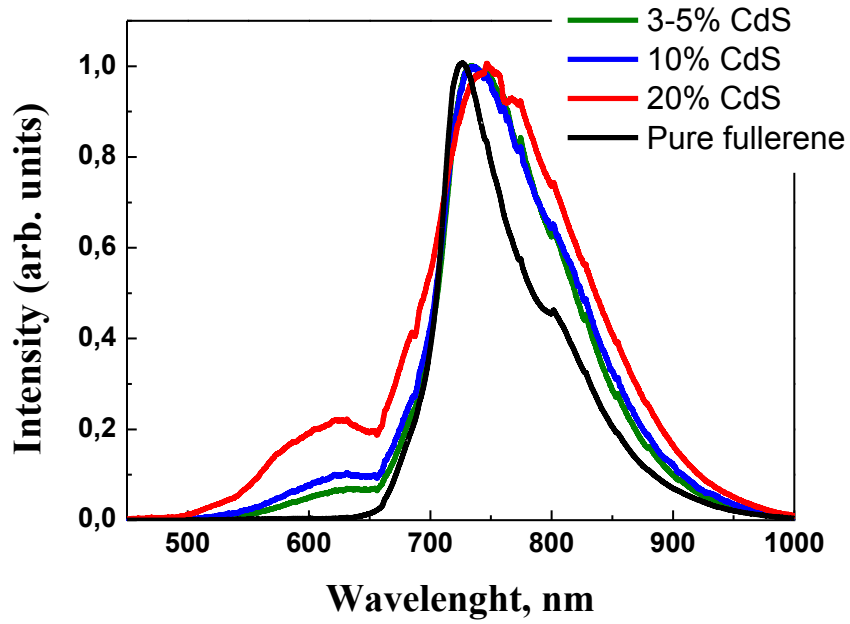

Figure 30. Photoluminescence spectra of C_{60}-CdS films obtained at 300 K. Measured with continuous laser excitation.

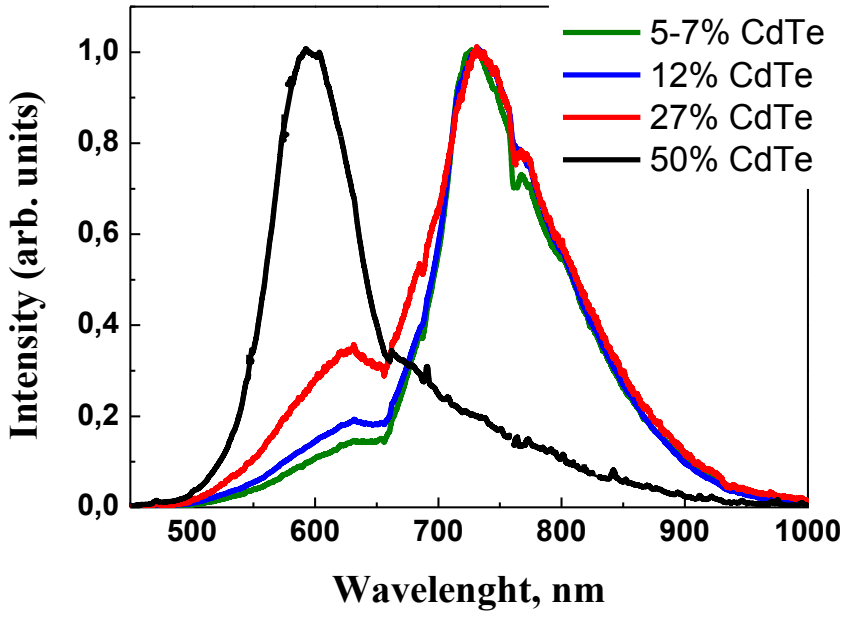

Figure 31. Photoluminescence spectra of C_{60}-CdTe films obtained at 300 K. The measurements were made with continuous laser excitation.

However C_{60} molecules and C_{60} complexes interaction is limited. Limitation is going from standing in crystal lattice. C_{60} toluene solution PL spectra presented a big additional peak at 650 nm and a small degree at 600 nm (see figure 29.). These values correspond to S_1-S_0 and

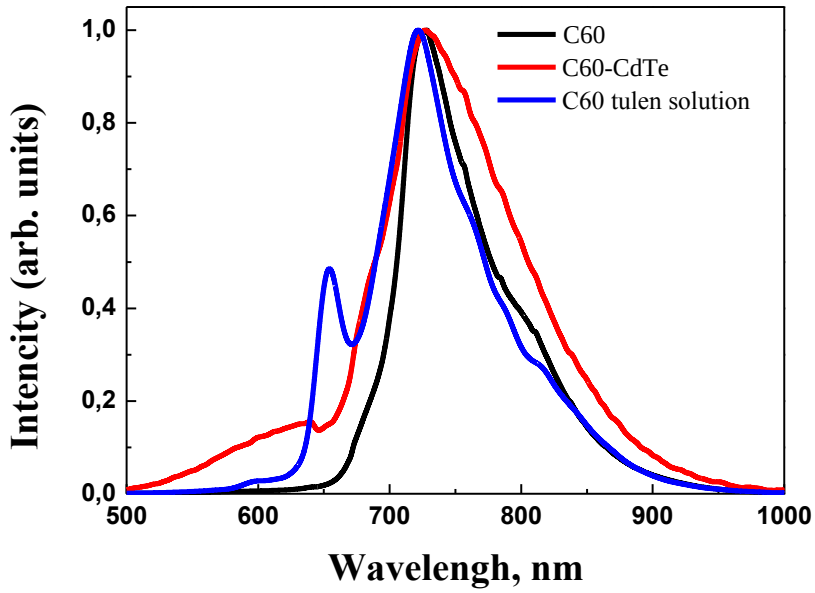

Figure 32. Photoluminescence spectra obtained at 300 K. Pure C_{60} spectrum is showed by black line. C_{60} with 50% CdTe is showed by red line. PL spectra of C_{60} toluene solution is showed by blue line. The measurements were made with continuous laser excitation.

S_2-S_0 fullerene transitions. It is possible because molecules in liquid phase are solvated by toluene and interact with each other, the degree of symmetry distortion increases and S_1-S_0 and S_2-S_0 transitions become permitted.

The resolution time of the installation with impulse laser and based on the MDR-2 monochromator is 10 ns. Time delay of signal measurement after the laser pulse is 90 ns. Thus, we see only a "fast" luminescence", on the spectrum. Consequently, the $T_1 \rightarrow S_1$ transitions with a large time constant did not give a significant contribution, and we can see the contribution of fluorescence. This is well illustrated by the 242 sample in Figure 30. The feature after the 750 nm - is fluorescence on the red spectra, which is confirmed by the literature data [Guangjun T. et al (2013)]. However, there is no 600 nm peak, which also explains the small time delay.

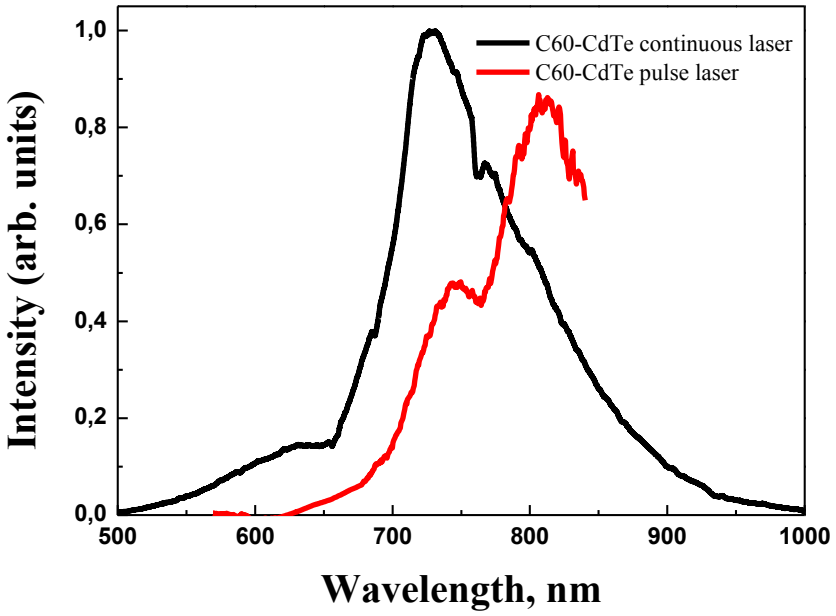

Figure 33. Photoluminescence spectra of 242 sample. Black line – is obtained by continuous laser excitation, red line – is obtained by impulse laser excitation.

a) b)

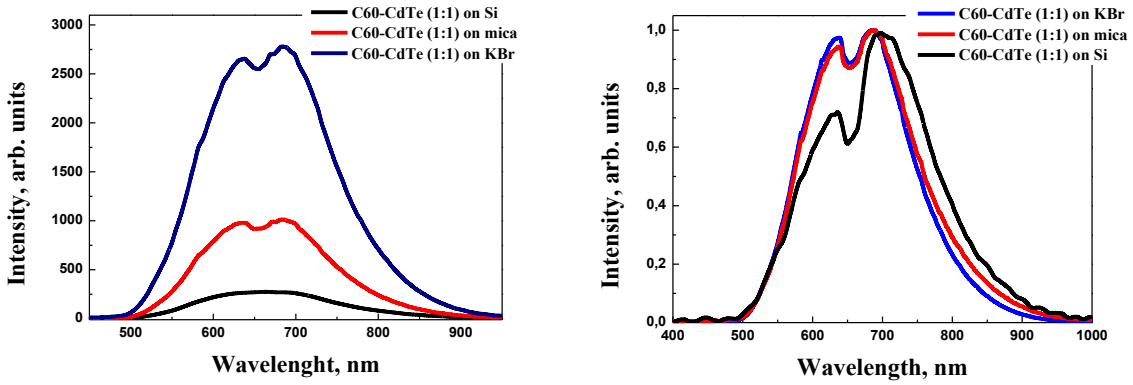

Figure 34. Photoluminescence spectra of the sample containing 50% of CdTe**.** a – intensity dependence, b- dependence of the 630 nm peak intensity. Black lines show spectra of sample on Si, red line is on mica, blue line is on KBr.

The photoluminescence dependence on the substrate influence was studied. It was found that PL intensity is different for the same samples deposed on different substrates. Figure 31 shows that the maximum intensity has the sample, which is deposited on KBr. Mica and KBr are fullerene-orienting substrates, allowing to grow crystal and polycrystalline structure.

Orienting properties of the substrate promotes to the formation of a larger number of C_{60}-CdTe molecular complexes, in the case of doped sample (see Figure 31, b). Thus extra peak intensity is bigger for films on mica and KBr.

The samples were subjected to X-ray irradiation in REIS-D equipment with a rhenium anode. X-ray energy flux was 5·10-3 J/s during 6 hour. PL spectra obtained at 300 K are shown in figure 32.

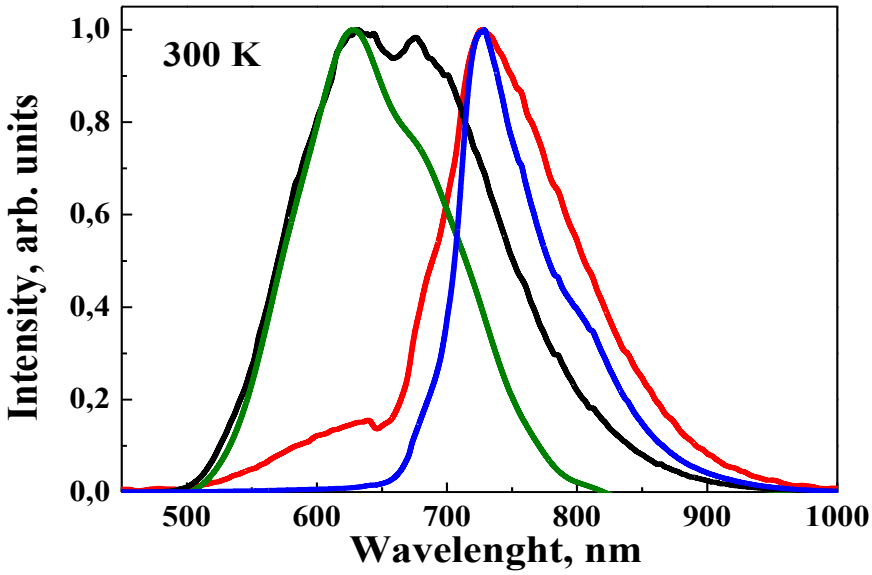

Figure 35. Photoluminescence spectra obtained at 300 K. X-ray irradiated pure C_{60} spectrum is shown by green line. X-ray irradiated C_{60} with 50% CdTe is shown by black line. Unexposed C_{60} with 50% CdTe and pure C_{60} PL spectra is red and blue line accordingly [Elistratova M. et al (2015)].

“The changes in PL spectra for irradiated CdTe-doped and pristine C_{60} films were investigated. The results have shown significant changes in the photoluminescence spectra after X-ray irradiation dose. A wide peak is observed only at 600−650 nm in the case of exposed samples. Therefore, after X-ray exposition the wide peak (T_1−T_0) at 730 nm disappears and another wide peak (S_1−S_0) emerges at 630 nm. T_1−T_0 is a transition between triplet fullerene levels and S_1−S_0 is a transition between singlet levels. More detailed information on the electronic structure comes from PL measurements at 77 K (see figure

33). One can see the weak peak at 630 nm in pristine fullerene films. The corresponding optical transition appears because the symmetry of fullerite is reduced at temperatures below 260 K and 90 K and a simple cubic lattice and glass phase are respectively formed. All additional peaks mentioned above are detected in X-ray exposed pristine fullerene. The energy position of the peaks does not change significantly but for 630 and 680 nm peaks the relative intensity increases after irradiation. In the case of composite films the changes are significantly stronger and initial emission peaks (730 nm and 820 nm) almost disappear. To explain the results, one can suggest that X-ray irradiation promotes dimerization in the fullerene matrix and reduces the symmetry, so that some optical transitions become possible." [Elistratova M. et al (2015)].

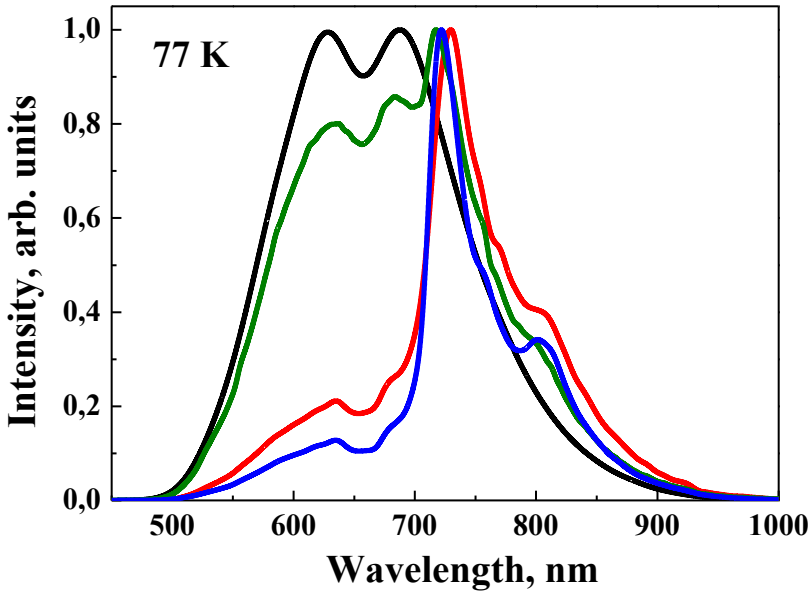

Figure 36. Photoluminescence spectra obtained at 77 K. X-ray irradiated pure C_{60} spectrum is shown by green line. X-ray irradiated C_{60} with 50% CdTe is shown by black line. Unexposed C_{60} with 50% CdTe and pure C_{60} PL spectra is blue and red line accordingly [Elistratova M. et al (2015)].

3.3 Quantum-chemical calculations

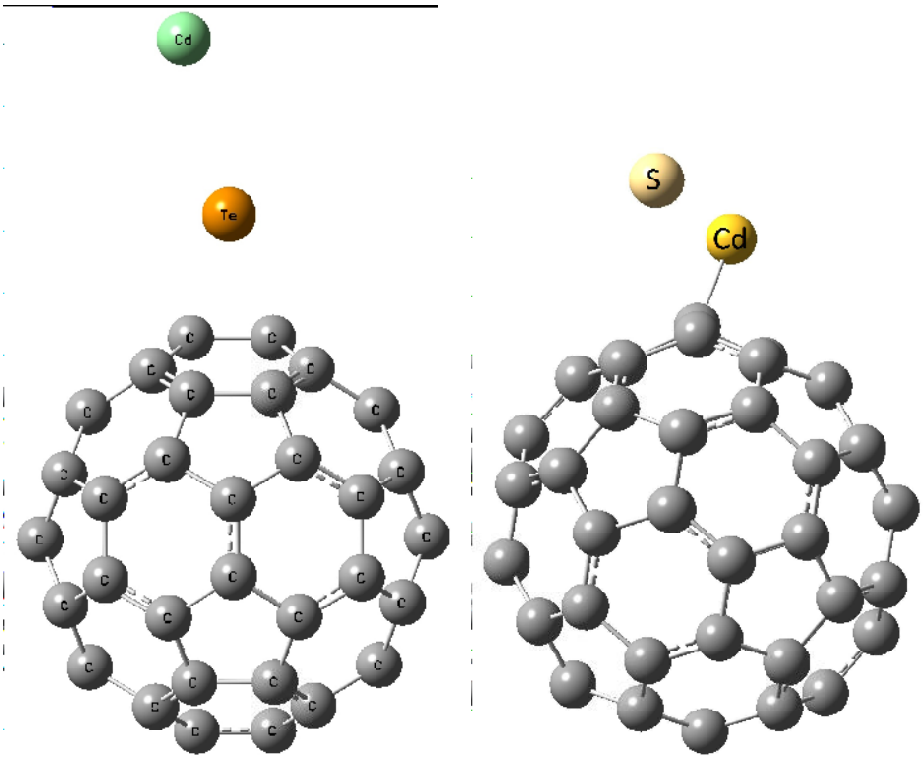

Figure 37. Optimal structure of C_{60}-CdS and C_{60}-CdTe molecular complexes.

Quantum chemical calculations of the optimum geometry, total energy and electronic structure of C_{60}-CdS and C_{60}-CdTe were performed by DFT-B3LYP method (see figure 34). Calculations showed that C_{60} and $<A_2B_6>$ form molecular complexes with bonding energy about 0.5 eV.

The energy spectrum of low-flying excited electronic states for linear and octahedral complexes were calculated (see figure 35). It was found that the symmetry lowering in the formation of complexes leads to the appearance of allowed singlet excitations in the electron spectrum, which are prohibited in the spectra of the original components. Different initial geometries, where the CdTe (CdS) molecule is parallel or (almost) perpendicular to the 5-6 or 6-6 fullerene bonds were optimized. Optimal geometries of C_{60}-CdS and C_{60}-CdTe molecular complexes are shown at figure 34. Calculations are in table 6. The energy of cluster formation is calculated under flowing conditions: $\Delta Ef = E\ (C_{60}CdChal) - E\ (C_{60}) - E\ (CdChal)$, where Chal = Te, S. Calculations show that the minimum energy structure has, where Chal atoms located above the 6-6 bond of the fullerene molecule at a distance of 2.2 Å for a C_{60}-CdTe cluster. In this case, Mayer bond order for Te atom with the nearest carbon

atoms is 0.54 and 0.60, for Cd is 0.16. To comparison, the bond order for C-C bond in fullerene is 1.38 for 6-6 bond, is 1.12 for 5-6 bond and 1.48 for or an isolated CdTe molecule. The total energy gain is 0.57 eV in the formation of this complex. HOMO-LUMO gap is equal 2.4 eV in the spectrum (for comparison, the calculation yields a molecule C_{60} HOMO-LUMO = 2.9 eV, and for molecules CdTe Eg = 1.3 eV).

Table 6. C_{60}-CdS and C_{60}-CdTe molecular complexes features. Results of QCC.

Complex	Symmetry (configuration)	Full energy, a.u.	Energy of complex formation, eV	Mayer bond order	HOMO-LUMO, eV
C_{60}CdTe	C_s (a)	-2448.5166	-0.572	C-Te: 0.60 Cd-Te: 0.16	2.4
	C_s (b)	-2448.5047	-0.334	C-Cd : 0.48 C-Te : 0.75 Cd-Te: 0.76	1.6
C_{60}CdS	C_s (a)	-2450.5831	-0.976	C-S: 0.67 Cd-S: 0.06	2.4
	C_s (b)	-2450.5743	-0.734	C-Cd : 0.50 C-Te : 0.72 Cd-Te: 0.73	1.6

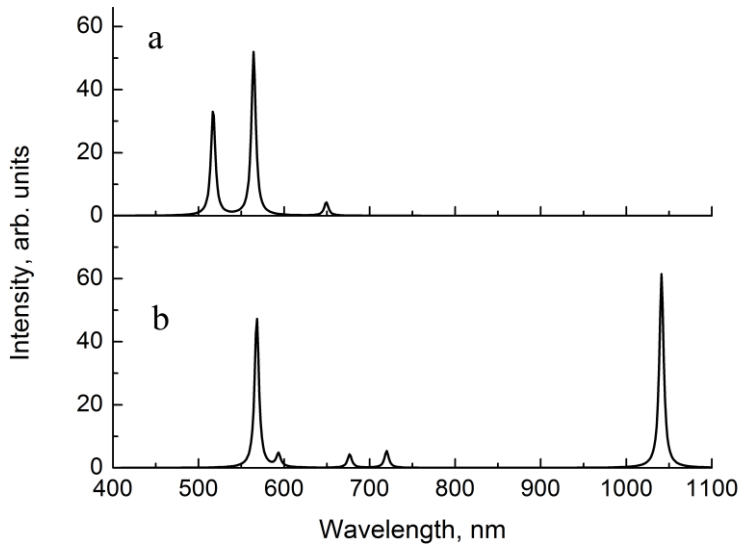

Figure 38. QCC results of excitation states calculations for C_{60}-CdTe complexes.

4 CONCLUSIONS

The main purpose of this work was to obtain and investigate new kind of material such as fullerene and to provide experimental and theoretical study.

The technological methods to obtain thin composite fullerene films was developed. Samples were investigated using optical spectroscopy technique (Scanning-electron microscopy, Atomic force microscopy, photoluminescence spectra measurements). Analysis of photoluminescence spectra in the context of substrate, dopants and amount of dopants influence were done. Moreover, X-ray exposing influence on fullerene film was also analyze.

Photoluminescence spectra results shown the appearance of extra peaks, related to the complex structures formation. Increase in amount of impurity led to formate more complexes and extra peak intensity increase.

It was shown that the type of substrate could change the spectra intensity due to the orientation properties on these surfaces. KBr and mica are orienting, and, consequently, films deposed on them have more intensity.

In this work were presented that x-ray exposing leads to significant changes in the structure of fullerene films with CdTe doping. Quantum-chemical calculations determined the appearance of dimers and oligomers in the C_{60} matrix. At low temperatures, pure C_{60} shows the existence of transitions from all energy levels, which means that in pure fullerene the S1-S0 transition, became permitted, due to the dimers formation and symmetry lowering. Fullerene doped by CdTe shows only the luminescence at 1.9 eV. Therefore, S_1-S_0 transitions dominate in spectrum.

In terms of practice, obtained results are important for forecasting properties and performance of thin fullerene films in complex test conditions. Practical importance also results on the study of the radiation resistance of nanocomposites and nanoparticles impact on their performance.

Bibliography

Agekyan V. F. 2000 Photoluminescence of semiconductor crystals. Sororus Journal 6(10), 101-107.

Bahshiev N. G. 1987. Introduction in molecular spectroscopy [Handbook]

Bang, J. H., & Kamat, P. V. 2011. CdSe quantum dot–fullerene hybrid nanocomposite for solar energy conversion: electron transfer and photoelectrochemistry. ACS nano, 5(12), 9421-9427.

Capozzia V., Santoro M., Perna G., Celentano G., Minafra A., Casamassima G.2001. Excitonic photoluminescence spectra of C60 single crystals grown by different techniques. The European Physical Journal AP, 77. 012503

Dennel G., Scharber M.C., Brabec C. J., 2009. Polymer-fullerene bulk-heterojunction solar cells. Adv. Mater. 21, 1323–1338

Drechsel, Frob H., 2008. Deposition of functional organic thin layers by means of vacuum evaporation// Vacuum‘s Best VIP, WILEY-VCH Verlog Gmbh & Co. KGaA, Weinheim, 7-11.

Elistratova, M., Romanov, N., Zakharova, I., & Kvyatkovskii, O. (2014, October). Optical spectroscopy of organic materials based on C60< A2B6>. In Journal of Physics: Conference Series (Vol. 541, No. 1, p. 012021). IOP Publishing.

Elistratova, M. A., Zakharova, I. B., & Romanov, N. M. (2015, January). X-ray radiation influence on photoluminescence spectra of composite thin films based on C60< CdTe>. In Journal of Physics: Conference Series (Vol. 586, No. 1, p. 012002). IOP Publishing.

Guangjun T., Yi Luo., 2013. Fluorescence and phosphorescence of single c60 molecules as stimulated by a scanning tunneling microscope. Angewandte Chemie., 125. 4914-4917

Hebard A. F., Zhou O., Zhoag Q., Fleming R. M., Haddon R. C. 1995. C_{60} films on surface-treated silicon: recipes for amorphous and crystalline growth**.** Thin Solid Films, 257. 147-153.

Gutsev G. L, Belay K. G., Weatherford C. A, Vasilets V. N, Anokhin E. M., Maksimychev A. V., Val'ba O. V., Martynenko V. M., Baskakov S. A., Leskova E. S., Shulga Y. M., 2011 Dimerization of defect fullerenes and the orientational phase transition in oxidized C60 fullerite. Nanosci. Nanotechnol. 11, 3. 1887-1896.

Hoppe H., Sariciftci N. S., 2005. Morphology of polymer/fullerene bulk heterojunction solar cells. J. Mater. Chem. 16, 45–61

Iwasa Y. T. Arima, R. M. Fleming, T. Siegrist, 0. Zhou, R. C. Haddon, L. J. Rothberg, K. B. Lyons, H. L. Carter Jr., A. F. Hebard, R. Tycko, G. Dabbagh, J. J. Krajewski, G. A. Thomas, T. Y. 1994. New phases of C60 synthesized at high pressure. Science, 264. 1570-1572.

Kano S., Kohno M., Sakiyama K., Sasaki S., Aya N. Shiraura H. 2003. Irradiation of CW-CO2 laser on a powder target. Formation of fullerene film from graphite powder. Chemical Physics Letters, 378. 474-480.

Katz E. A. 2008. Semiconducting fullerene-based materials for the direct conversion of solar energy into electricity (review). P. 3. General features of various fullerene-based photovoltaic cells. Inorganic C60-based solar cells. Journal of functional material, 2, 4. 143-152

Katz E. A., Faiman D., Shtutina S., Isakina A.,Vagotintscv K., Iakoubovskii K. High Quality Textured C60 Thin Films on a Mica Substrate: Growth, Crystalline Structure, Electrical and Photoelectric Properties» // Solid State Phenomena. -2001. -V. 80. p. 15-20.

Katz E. A., Faiman D., Slitutina S., Isaklna A. 2000. Deposition and structural characterization of high quality textured C_{60}. Thin Solid Films. 368, 49-54.

Kazaoui S., Minami N., Tanabe. 1998. Comprehensive analysis of intermolecular charge-transfer excited states in C60 and C70 films. Physical Review B. 58. 7689

Kognovitski S. O., Nashchekin A. V., Sokolov R. V., Soshnikov I. P., Konnikov S. G., 2003. Fullerene-containing C60–CdTe(CdSe) composite nanostructures. Technical Physics Letters, 29, 6. 477–479.

Koh H., Lee J., 2009 Well-Organized CdS/C_{60} in Block Copolymer Micellar Cores. Macromolecular Rapid Communications, 30. 976-980

Klesper H., Baumann R., Bargon J., Hormes J., Zumaq H., Kohring A. 2005. Investigations on the behavior of C60 as a resist in X-ray lithography. Applied Physics A, 80. 1469–1479.

Li L., Tang, Q., Li, H., & Hu, W. 2008. Molecular orientation and interface compatibility for high performance organic thin film transistor based on vanadyl phthalocyanine. The Journal of Physical Chemistry B, 112(34), 10405-10410.

Lee J. K., Ma W.L., Brabec C. J., Yuen J., Moon J. S., Kim J. Y., Lee K., Bazan G. C., Heeger A. 2008. J. Processing additives for improved efficiency from bulk heterojunction solar cells J. Am. Chem. Soc., 130, 3619-3623

Makarova T. L. 2001. Electrical and optical properties of pristine and polymerized fullerenes. Semiconductors 35, 3. 243–278.

Nikolaev A. V., Bodrenko I. V., Tkalya E. V. 2008. Theoretical study of molecular electronic excitations and optical transitions of C60. Physical Review A, 77. 012503

Robinson A. P. G., Palmer R. E., Tada T., Kanayama T., Preece J. A. 1996. A Fullerene derivative as an electron beam resist for nanolithography. Applied Physics Letters, 72. 1302

Pakhomov, G. L., Travkin, V. V., Luk'yanov, A. Y., Stakhira, P. I., & Kostiv, N. V. 2013. Thin-film photovoltaic cells based on vanadyl phthalocyanine and fullerene. Technical Physics, 58(2), 223-230.

Pan L., Ishikawa A., Tamai N. 2007. Detection of optical trapping of CdTe quantum dots by two-photon-induced luminescence. Phys. Rev. B, 5. 161305.

Stijn De Vusser, Soeren S., Myny K., Genoe J., Heremans P., 2006. Low voltage complementary organic inverters. Applied Physics Letters, 88. 103501.

Sakai S., Mitani S., Sugai I., Takanashi K., Matsumoto Y., Entani S.,. Naramoto H, Avramov P., Maeda Y. 2011. Effect of cotunneling and spin polarization on the large tunneling magnetoresistance effect in granular C60-Co films. Physical review B, 83. 174422.

Scharber, M. C., Mühlbacher, D., Koppe, M., Denk, P., Waldauf, C., Heeger, A. J., Brabec, C. J. 2006. Design rules for donors in bulk-heterojunction solar cells—Towards 10% energy-conversion efficiency. Advanced Materials, 18(6), 789-794.

Shibu, E. S., Sonoda, A., Tao, Z., Feng, Q., Furube, A., Masuo, S., ... & Biju, V. 2012. Photofabrication of fullerene-shelled quantum dots supramolecular nanoparticles for solar energy harvesting. ACS nano, 6(2), 1601-1608.

Suzuki A., Nishimura K., Oku T. 2014. Effects of germanium tetrabromide addition to zinc tetraphenyl porphyrin / fullerene bulk heterojunction solar cells. Electronics, 3. 112-121.

Takeda A., Oku T., Suzuki A., Kikuchi K., Kikuchi S., 2009. Fabrication and characterization of inorganic-organic hybrid solar cells based on CuInS2 // Journal of the Ceramic Society of Japan, 117. 967–969.

Tsang S. W., Fu H., Wang R., Lu J., Yu K., Tao Y.. 2009. Highly efficient cross-linked PbS nanocrystal/C-60 hybrid heterojunction photovoltaic cells. Applied Physics Letters, 95. 183505.

Zakharova I. B., Ziminov V. M., Nashchekin A. V., Vainshtein Yu. S., Aleshin A. N. 2003. Optical spectroscopy of thin C60:CdS composite films. Semiconductors, 47, 1. 105–109.

Zauco A., Sobral H., Basiuk E.V., Saniger-Blesa J.M., Muniz M. V. 2005. Polymerization of C60 fullerene thin films by UV pulsed laser irradiation Applied Surface Science, 248. 243‑247.

Zhugayevych A., Postupna O., Tretiak S., Bazan G., 2012. Understanding the high device efficiency of a class of solution-processed small-molecule solar cells. Proceedings on APS March Meeting № Y49.005